JEM Journal of Experimental Medicine

ARTICLE

Inhibition of astrocytic DRD2 suppresses CNS inflammation in an animal model of multiple sclerosis

Shen-zhao Lu[1*], Yue Wu[1*], Yong-shun Guo[1*], Pei-zhou Liang[1*], Shu Yin[1*], Yan-qing Yin[1], Xiu-li Zhang[3], Yan-Fang Liu[3], Hong-yan Wang[4], Yi-chuan Xiao[5], Xin-miao Liang[3], and Jia-wei Zhou[1,2,6,7]

Astrocyte activation is associated with progressive inflammatory demyelination in multiple sclerosis (MS). The molecular mechanisms underlying astrocyte activation remain incompletely understood. Recent studies have suggested that classical neurotransmitter receptors are implicated in the modulation of brain innate immunity. We investigated the role of dopamine signaling in the process of astrocyte activation. Here, we show the upregulation of dopamine D2 receptor (DRD2) in reactive astrocytes in MS brain and noncanonical role of astrocytic DRD2 in MS pathogenesis. Mice deficient in astrocytic *Drd2* exhibit a remarkable suppression of reactive astrocytes and amelioration of experimental autoimmune encephalomyelitis (EAE). Mechanistically, DRD2 regulates the expression of 6-pyruvoyl-tetrahydropterin synthase, which modulates NF-κB activity through protein kinase C-δ. Pharmacological blockade of astrocytic DRD2 with a DRD2 antagonist dehydrocorybulbine remarkably inhibits the inflammatory response in mice lacking neuronal *Drd2*. Together, our findings reveal previously an uncharted role for DRD2 in astrocyte activation during EAE-associated CNS inflammation. Its therapeutic inhibition may provide a potent lever to alleviate autoimmune diseases.

Introduction

Multiple sclerosis (MS) is an immune-mediated disease in the central nervous system (CNS), which is characterized by chronic and progressive inflammation, demyelination, and neurodegeneration (Reich et al., 2018). Many patients are at first diagnosed with a relapsing–remitting form of the disease, which likely progresses into a second phase, secondary progressive MS. Although there are more than a dozen disease-modifying drugs available for MS treatment, the efficacy of these treatments remains limited. Emerging evidence has suggested that the deregulated CNS innate immunity plays crucial roles on the onset and progression of the disease (Baecher-Allan et al., 2018; Wheeler et al., 2020). Understanding of this highly complex process remains very limited. Therefore, it is critical to identify and characterize the cellular and molecular basis of disrupted CNS innate immunity in MS that provides a new avenue for the intervention of the disease progression.

Astrocytes, the most abundant cell type in the CNS, play essential roles in the maintenance of CNS homeostasis, including energy metabolism, neurotransmission, regulation of innate immunity, and the blood–brain barrier (BBB) formation (Sofroniew and Vinters, 2010; Sofroniew, 2020). In the context of MS/experimental autoimmune encephalomyelitis (EAE), astrocyte activation is one of prominent pathological features in each stage of the disease. Many of their normal functions are significantly perturbed (Reich et al., 2018; Wheeler and Quintana, 2019; Baecher-Allan et al., 2018), and activated astrocytes are detrimental to proper neural function (Wheeler and Quintana, 2019; Wheeler et al., 2020). Reactive astrocytes contribute significantly to the BBB disruption, secretion of inflammatory cytokines, and recruitment of peripheral immune cells into the brain parenchyma. However, the molecular mechanisms underlying astrocyte activation and its

[1]Institute of Neuroscience, State Key Laboratory of Neuroscience, CAS Center for Excellence in Brain Science and Intelligence Technology, Chinese Academy of Sciences, Shanghai, China; [2]School of Future Technology, University of Chinese Academy of Sciences, Beijing, China; [3]CAS Key Laboratory of Separation Science for Analytical Chemistry, Dalian Institute of Chemical Physics, Chinese Academy of Sciences, Dalian, China; [4]State Key Laboratory of Cell Biology, Key Laboratory of Systems Biology, CAS Center for Excellence in Molecular Cell Science, Shanghai Institute of Biochemistry and Cell Biology, Chinese Academy of Sciences, University of Chinese Academy of Sciences, Innovation Center for Cell Signaling Network, Shanghai, China; [5]The Key Laboratory of Stem Cell Biology, Institute of Health Sciences, Shanghai Institutes for Biological Sciences, Chinese Academy of Sciences, University of Chinese Academy of Sciences, Shanghai, China; [6]Shanghai Center for Brain Science and Brain-Inspired Intelligence Technology, Shanghai, China; [7]Co-innovation Center of Neuroregeneration, School of Medicine, Nantong University, Nantong, Jiangsu, China.

*S.-z. Lu, Y. Wu, Y.-s. Guo, P.-z. Liang, and S. Yin contributed equally to this paper. Correspondence to Jia-wei Zho: jwzhou@ion.ac.cn; Xin-miao Liang: liangxm@dicp.ac.cn.

contribution to MS pathogenesis remain incompletely understood.

Classical neurotransmitter dopamine (DA) has been known to play an important role in a variety of brain activities, such as motor function, motivation, and cognition. The complex function of DA is believed to be associated with wide distribution of five dopamine receptors, DRD1–DRD5, in a variety of tissue and organs. Recent studies have implicated the involvement of dopaminergic (DAergic) system in MS. Fatigue is a very common symptom in MS (Walker et al., 2012). Neuroimaging studies in MS patients with fatigue have shown reduced structural integrity or increased white matter pathology in the regions of the mesocorticolimbic pathway, such as the ventromedial prefrontal cortex (PFC) and striatum, the regions that are heavily innervated by DAergic terminals, indicating deregulated DAergic neurotransmission in MS (Dobryakova et al., 2013; Pardini et al., 2010). Functional neuroimaging studies have further revealed lower levels of glucose metabolism or reduced connectivity in the PFC and striatum of MS individuals who have high fatigue, suggesting an impaired functionality of the mesocorticolimbic pathway in MS (Engstrom et al., 2013; Dobryakova et al., 2015). However, the role of DA system in MS pathogenesis remains largely elusive.

Recent studies have shown that in the CNS, glial cells such as astrocytes and microglia express DA receptors in addition to neuronal cells (Shao et al., 2013; Zhu et al., 2018), suggesting new regulatory mechanisms or novel role for DAergic neurotransmission that has been overlooked in the past years. Interestingly, DRD2, but not other DRD2-like subfamily members DRD3 or DRD4, is strongly expressed in white matter fibrous astrocytes in the human brain (Mladinov et al., 2010), providing a molecular basis for DRD2-dependent regulation of CNS innate immunity and associated demyelinating diseases. Indeed, deficiency of astrocytic DRD2 (aDRD2) promotes neuroinflammation and DA neuron degeneration in animal model of Parkinson's disease (Shao et al., 2013; Zhu et al., 2018). Given these points, we hypothesized that DRD2 signaling in astrocytes influences disease progression and pathology in MS/EAE.

In the present study, we aim to unravel the role of activated astrocytes and its regulation in the pathogenesis of EAE, an animal model of MS. We reveal the DRD2/6-pyruvoyl-tetrahydropterin synthase (PTS)–dependent mechanism for astrocyte-driven CNS inflammation as a crucial signaling pathway in the regulation of pathogenesis of EAE, possibly also in MS. We show that preferential ablation of *Drd2* or *PTS* in astrocytes leads to a dramatic reduction in the severity of the disease, which is accompanied by substantially reduced production of proinflammatory mediators in the spinal cord. Our data indicate that aDRD2 signaling is essential for the control of CNS inflammation and neurodegeneration in EAE in DA-independent manner.

Results

Altered expression of DRD2 in MS brain

To investigate the expression of DRD2 in brain tissue of patients with MS, we performed immunoblotting analysis and found that there was a marked increase in expression levels of DRD2, which was positively correlated with levels of components of the NF-κB signaling pathway, such as phospho-IκB kinase (IKK)α/β, IKKα/β, phospho-p65, p65, and iNOS (Fig. 1, A and B; and Table S1). A previous study showed that DRD2 is strongly expressed in the white matter fibrous astrocytes and in layer I protoplasmic astrocytes in the PFC of human brain (Mladinov et al., 2010). In agreement with this finding, there was a trend toward the increase in DRD2 immunoreactivity in GFAP$^+$ (glial fibrillary acidic protein promoter) astrocytes in the normal-appearing white matter in MS brain compared to control (Fig. 1, C and D; and Table S2). Notably, the cells that were double-labeled with anti-DRD2 and GFAP antibodies and showed intact cell morphology within the active or chronic lesion sites were sparse, indicating poor survival of these cells (data not shown).

Next, we determined DRD2 expression in EAE, a mouse model of MS at various time points following EAE induction. Expression of DRD2 in the white matter of the spinal cord of wild-type mice was markedly increased at day 12 and 17 after EAE induction compared with untreated (Fig. 1, E and F). Notably, some of these DRD2 immunosignals were confined in GFAP$^+$ cells. In contrast, there was no significant alteration in DRD2 immunoreactivity in the gray matter of the spinal cord of wild-type mice at various stages following EAE induction (Fig. 1, E and G). These data suggest a role for DRD2 in the white matter astrocytes during CNS neuroinflammation in EAE.

Selective deficiency of *Drd2* in astrocytes dramatically attenuates EAE

To assess whether aDRD2 influences the course of EAE, we removed *Drd2* selectively in astrocytes by generating astrocyte-specific *Drd2*-deficient mice, *Drd2$^{flox/flox}$; mGFAP-Cre* (hereafter referred to as *Drd2^{mGFAP}*). EAE was induced in these conditional KO (cKO) mice by active immunization with MOG_{35-55}. The astrocyte-specific *Drd2*-null mice exhibited remarkable resistance to EAE compared to their littermate control, as manifested by a significant delay in the onset of the disease and profound reduction in disease severity (Fig. 2 A). In contrast, deletion of DAR subtype *DRD4*, which also belongs to dopamine D2-like receptor subfamily (Beaulieu and Gainetdinov, 2011), selectively in astrocytes did not result in a significant alteration in EAE severity (Fig. 1 B), which is in a good agreement with previous finding that DRD4 is not expressed in white matter fibrous astrocytes in the PFC (Mladinov et al., 2010). These data show a DAR subtype specificity for the DRD2-dependent regulation of CNS innate immunity.

Traditionally, DRD2 has been known to be abundantly expressed in neuronal cells (Beaulieu and Gainetdinov, 2011). To determine the potential role of neuronal *Drd2* during EAE, we bred *Drd2$^{flox/flox}$* mice with murine thymocyte antigen 1 (Thy1)-Cre transgenes (Campsall et al., 2002). Mice lacking *Drd2* in neuronal cells (*Drd2^{Thy1}*) exhibited no significant difference in neurobehavioral deficits and pathology upon challenge with MOG_{35-55} immunization when compared with their littermate control (Fig. 2 C and Fig. S1). Moreover, previous studies have demonstrated a crucial role of CD4$^+$ T cells in EAE pathogenesis (Miller and Karpus, 2007). Naive CD4$^+$ T cells expressing both DRD1 and DRD2 are involved in the regulation of cytokine

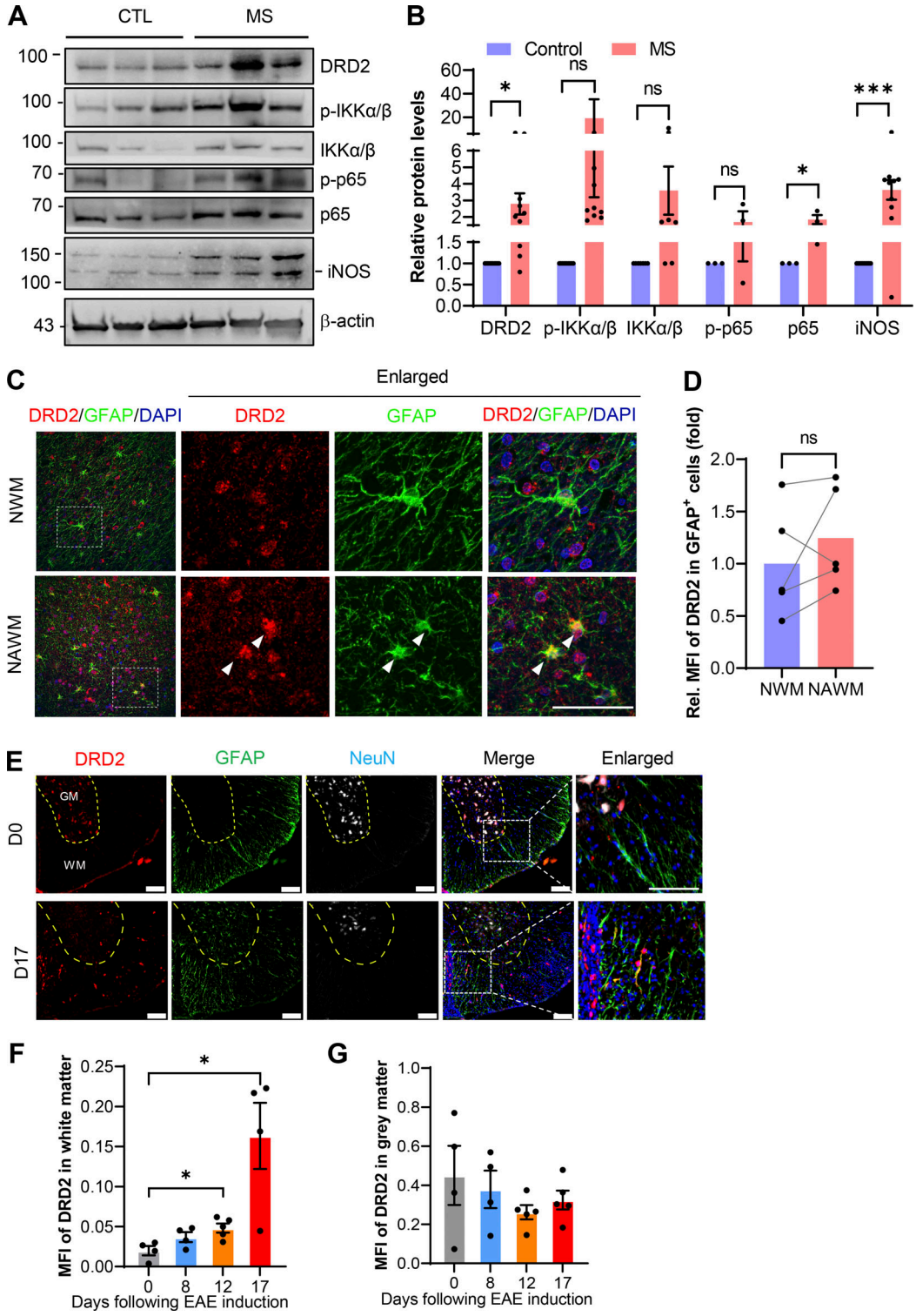

Figure 1. **Expression of DRD2 and NF-κB–signaling proteins is upregulated in the white matter of brain of patients with MS or in the spinal cord of EAE. (A and B)** Representative immunoblots showing expression of DRD2 and phospho-IKKα/β, phospho-p65 and their nonphosphorylated forms (A) and quantitative data (B). *n* = 7. Molecular weight measurements are shown in kilodaltons. **(C and D)** Representative immunofluorescent microphotographs showing DRD2$^+$ astrocytes in the normal-appearing white matter of brain from patients with MS (*n* = 5) and control individuals (*n* = 4). The box in each image outlines the area enlarged to the right. Quantitative data of C are shown in D. Scale bars, 50 µm. **(E)** Representative immunofluorescent histochemical staining for DRD2, GFAP, and NeuN on the spinal cord of wild-type mice during EAE (*n* = 4–5). The box in each image outlines the area enlarged to the right. GM, gray matter; WM, white matter. Scale bars, 100 µm. **(F and G)** Quantitative data of DRD2 expression levels in the white matter (F) or gray matter (G) shown in E. NWM, normal white matter; NAWM, normally appearing white matter. Data are represented as mean ± SEM. P values are from unpaired *t* tests, in which ns (not significant) indicates P > 0.05. *, P < 0.05; ***, P < 0.001.

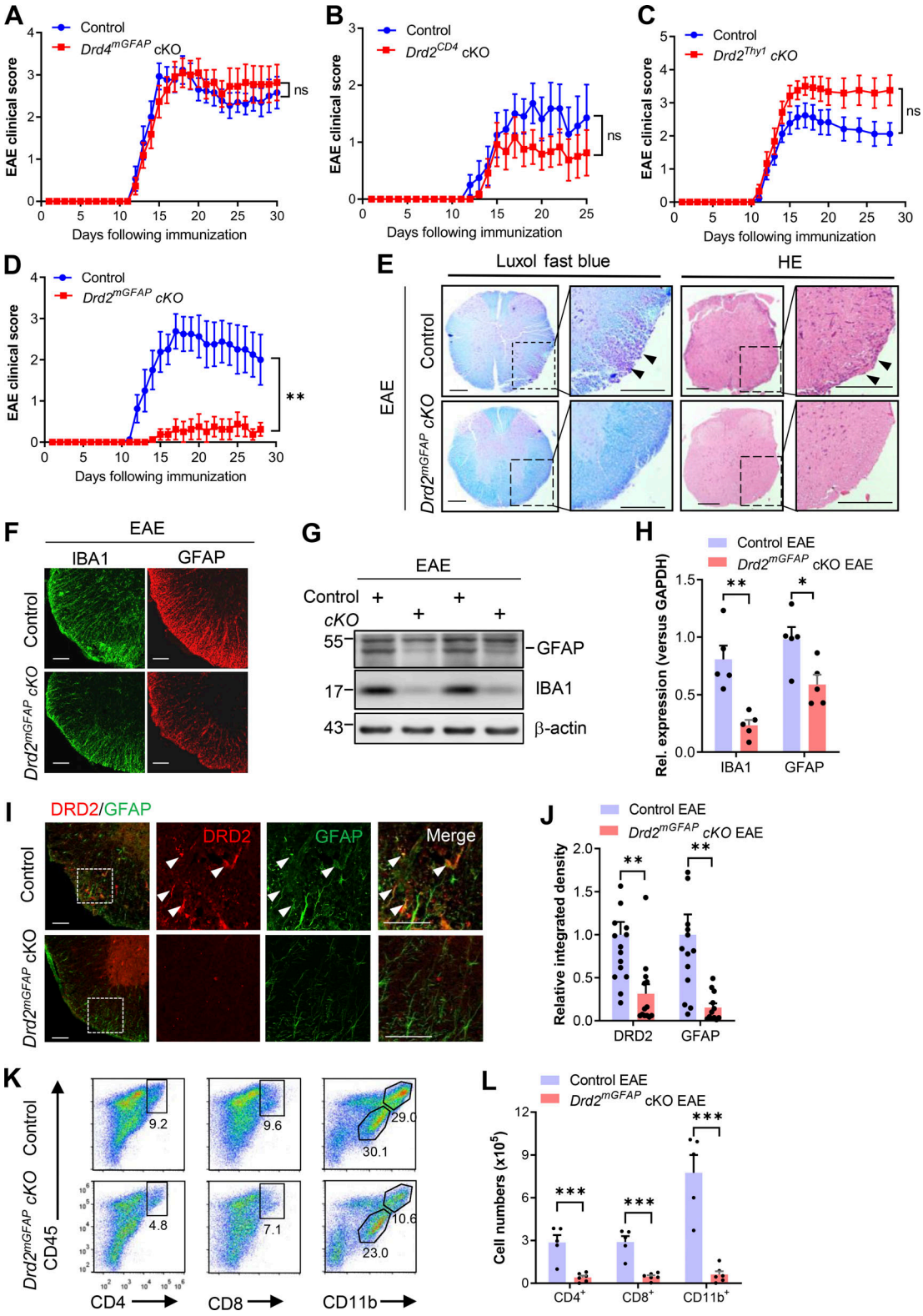

Figure 2. **Selective ablation of *Drd2* in astrocytes, but not in neuronal cells, ameliorates EAE. (A)** Representative graph showing average clinical scores of age-matched female *Drd2*^{mGFAP} cKO mice and control subjected to EAE. *n* = 8 mice per group. **(B)** Representative graph showing average clinical scores of age-matched female *Drd4*^{mGFAP} cKO mice and control subjected to EAE. *n* = 11 mice for cKO; *n* = 13 mice for control. **(C)** Representative graph showing average clinical scores of age-matched female *Drd2*^{Thy1} cKO mice and control subjected to EAE. *n* = 12 mice for cKO; *n* = 17 mice for control. **(D)** Representative graph showing average clinical scores of age-matched female *Drd2*^{CD4} cKO mice and control subjected to EAE. *n* = 12 mice per group. **(E)** Luxol fast blue staining and hematoxylin and eosin (HE) staining on the spinal cord sections from *Drd2*^{mGFAP} cKO mice and control on day 17 after EAE induction are shown. Inflammatory cell infiltration and demyelination are indicated with arrowheads. Inserts are enlarged views of the ventral part of the spinal cord of the corresponding photos.

Scale bars, 200 mm. **(F)** Immunofluorescent histochemical staining for IBA1 and GFAP on the spinal cord of *Drd2*^{mGFAP} cKO mice and control on day 17 following EAE induction are shown. Scale bars, 75 mm. **(G)** Representative Western blots showing GFAP and IBA1 expression in the spinal cord of *Drd2*^{mGFAP} cKO mice and control animals. **(H)** Quantitative data shown in G. *n* = 5 per group. **(I)** Immunofluorescent histochemical staining for DRD2 and GFAP on the spinal cord of *Drd2*^{mGFAP} cKO mice and control on day 17 during EAE. Right panels are enlarged views of the dashed areas. Scale bars, 100 mm. The arrowhead points to the cells with co-expression of GFAP and DRD2. **(J)** Quantitative data shown in I. Control EAE, *n* = 5; *Drd2*^{mGFAP} cKO EAE, *n* = 4 mice. **(K)** Cytometric analysis of immune cells (CD45$^+$) infiltrates from the spinal cord and brain of *Drd2*^{mGFAP} cKO mice and control 17 d after immunization with MOG_{35-55}. The gating strategy is shown in Fig. S3. **(L)** Quantitative data shown in K. Control EAE, *n* = 5 mice, *Drd2*^{mGFAP} cKO EAE, *n* = 6 mice. Data are represented as mean ± SEM. P values are from unpaired *t* tests (H, J, and L) or two-way ANOVA (A–C), in which ns (not significant) indicates P > 0.05. *, P < 0.05; **, P < 0.01; and ***, P < 0.001.

production in T cells (Pacheco et al., 2009; Besser et al., 2005). But the role of DRD2 in CD4$^+$ cells during EAE is not known. We found that CD4$^+$ T cell–specific *Drd2* removal did not influence the EAE phenotype as compared with their littermate control (Fig. 2 D), indicating that DRD2 in CD4$^+$ T cells is not involved in EAE course. Collectively, these data suggest that aDRD2 plays a distinct role from its counterparts in neurons or CD4$^+$ T cells with respect to the CNS inflammatory response during EAE.

Reduced inflammatory response exclusively in the CNS of *Drd2*^{mGFAP} cKO mice

Consistent with the reduced clinical EAE phenotype, the demyelination and inflammatory infiltration in the spinal cord were greatly suppressed in *Drd2*^{mGFAP} cKO mice, as assessed by Luxol fast blue staining and hematoxylin and eosin staining (Fig. 2 E). These were accompanied by a remarkable attenuation of the activation of GFAP$^+$ astrocytes and IBA1$^+$ microglia in the white matter, as revealed by immunohistochemistry and Western blot analysis (Fig. 2, F–H). As expected, the intensity of DRD2 immunosignals in GFAP$^+$ fibrous astrocytes in the white matter was dramatically reduced in *Drd2*^{mGFAP} cKO mice (Fig. 2, I and J), which occurred concurrently with pronounced decreases in levels of inflammatory genes and chemokines involved in the recruitment of immune cells, such as *Ccl2*, *Ccl20*, *Il-6*, *Cxcl1*, *Cxcl2*, *Cxcl9*, *Cxcl10*, and *Tnf-α*, in the spinal cord of *Drd2*^{mGFAP} cKO mice when compared to their wild-type counterparts (Fig. S2 A). In addition, the levels of *Mmp3*, and *Spp1* (also known as *Opn*, encoding osteopontin) which are associated with EAE and MS pathology (Chabas et al., 2001; Hur et al., 2007; Mayo et al., 2014; Mirshafiey et al., 2014; Traugott, 1987), were reduced in *Drd2*^{mGFAP} cKO mice (Fig. S2 A), indicating that aDRD2 may be also associated with adaptive immunity during EAE. Notably, there was no significant difference in the infiltration of inflammatory cells, such as IBA1$^+$, CD22$^+$, CD8$^+$, or CD4$^+$ cells in the leptomeninges of the spinal cord between genotypes following EAE induction (Fig. S2, B and C). Together, these data suggest that aDRD2 deficiency is associated with dramatically ameliorated CNS immune response and largely suppressed EAE.

Further FACS analysis revealed a substantial reduction in mononuclear cell infiltrates, such as CD4$^+$ cells, CD8$^+$ cells, and neutrophils, in the CNS of *Drd2*^{mGFAP} cKO mice at the peak of the disease after EAE induction compared to control animals (Fig. 2, K and L; and Fig. S3 A). In sharp contrast, there was an explosive inflammatory response in the peripheral immune system in *Drd2*^{mGFAP} cKO mice that was comparable to control, as manifested by huge increases in the number of inflammatory cells in the draining lymph nodes and spleen, which showed no significant difference between genotypes at the peak of the disease (Fig. S3, A–C). No marked difference in mRNA levels of inflammatory mediators was observed in the draining lymph nodes between genotypes before the onset of EAE (Fig. S3 D). These results suggest that the resistance of *Drd2*^{mGFAP} cKO mice to EAE likely occurs in the CNS, but not in the peripheral immune system. Hence, aDRD2 is key to maintain the balance of CNS innate immunity in EAE.

Deficiency of a*Drd2* leads to the suppression of proinflammatory response

To unravel the aDRD2-regulated molecular events in response to EAE, we carried out RNA sequencing (RNA-seq) analysis on the spinal cord tissue at the peak of the disease following EAE induction. Analysis of differentially expressed genes between *Drd2*^{mGFAP} cKO EAE and control EAE showed 1,538 upregulated and 2,069 downregulated genes (P < 0.05, fold change >1.5) among all the detected genes (Fig. 3 A). Hierarchical clustering showed that expression of genes associated with NF-κB signaling pathway, such as *Nfkb2*, *Myd88*, *Lbp*, *Il1b*, *Traf2*, and *Traf5*, which are necessary for autoimmune diseases (van Loo et al., 2006), were dramatically downregulated by aDRD2 deficiency (right panel in Fig. 3 B; and Fig. S4, A and B). Consistently, Kyoto Encyclopedia of Genes and Genomes (KEGG) enrichment analysis of biological processes showed that the top 20 listed pathways of downregulated genes were related to NF-κB signaling, infection, and immunological responses (Fig. S4 C). Gene set enrichment analysis (GSEA) showed that *Drd2*^{mGFAP} cKO mice exhibited decreased activation of pathways associated with the inflammatory response in EAE and MS, including cytokine–cytokine receptor interaction (van Loo et al., 2006; Kang et al., 2013), IFN-γ signaling (Reich et al., 2018), immunoregulatory interactions, and initial triggering of complement (Liddelow et al., 2017; Fig. 3 C). In contrast, most of the top listed pathways of the upregulated genes in KEGG or GSEA were related to neurotransmission and dendritic spine maintenance (Fig. 3 C and Fig. S4 D). Interestingly, consistent with previous finding that mice lacking AQP4 display remarkably less severe EAE (Li et al., 2009), we found that there was a significant reduction of AQP4 mRNA levels in *Drd2*^{mGFAP} cKO mice with EAE, compared with wild-type EAE mice (Fig. 3 D), supporting an idea that AQP4 is involved in CNS inflammation.

To validate whether *Drd2* deficiency in astrocytes causes the suppression of inflammatory response, we performed DNA microarray analysis on the astrocytes isolated from the spinal cord of *Drd2* cKO EAE mice on the peak of the disease by using magnetic-activated cell sorting based on antibody against glutamate aspartate transporter (GLAST). This strategy allowed for precise identification of molecular signaling cascades occurred

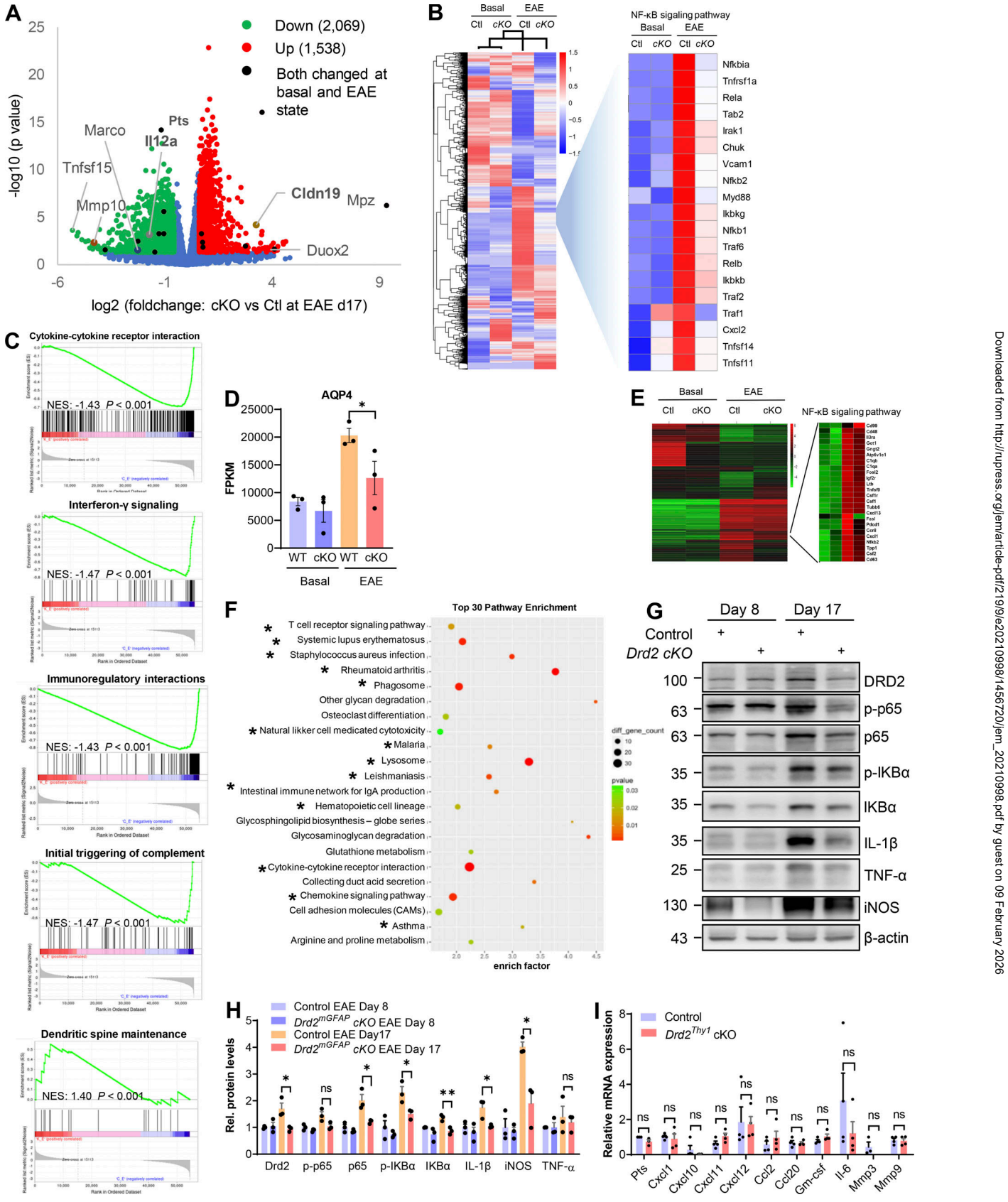

Figure 3. **Selective deficiency of *Drd2* in astrocytes limits NF-κB activation. (A)** Volcano plot showing the results of differential gene expression analysis in the spinal cord tissue between *Drd2*^{mGFAP} cKO and control mice under either basal condition or EAE on day 17 after immunization. *n* = 3 mice per group. **(B)** The heatmap of differentially expressed genes with adjusted P values <0.05 and $\log_2$ fold-change >1.2 from RNA-seq analysis of *Drd2*^{mGFAP} cKO and control mice

under either basal condition or EAE on day 17 after immunization. *n* = 3 mice per group. **(C)** GSEA analysis of RNA-seq data obtained from the spinal cord tissue of *Drd2*^{mGFAP} cKO versus control mice during EAE. **(D)** The FPKM (fragments per kilobase of exon model per million mapped fragments) values of *Aqp4* gene in the spinal cord tissue of *Drd2*^{mGFAP} cKO and control mice on day 17 after immunization, revealed by RNA-seq analysis. *n* = 3 mice per group. **(E and F)** Ablation of *Drd2* in astrocytes suppresses the activation of NF-κB signaling in EAE. **(E)** Hierarchical clustering of genes differentially expressed in Glast^{+} astrocytes between female *Drd2*^{mGFAP} cKO and littermate control with or without EAE induction. Glast^{+} astrocytes are isolated from the spinal cord using magnetic-activated cell sorting on day 17 following EAE induction. **(F)** The top 30 differentially regulated KEGG pathways. Asterisks indicate the 14 functional categories that are related to the immune response. **(G and H)** Western blot analysis of tissue lysates from the spinal cord of *Drd2*^{mGFAP} cKO mice and control on 8 and 17 d after EAE induction (G) and quantitative data (H). *n* = 3. **(I)** Representative graph showing relative mRNA levels of pro-/anti-inflammatory mediators in 2-mo-old *Drd2*^{Thy1} cKO and control animals. *n* = 3–4. Data are represented as mean ± SEM. P values are from unpaired *t* tests, in which ns (not significant) indicates P > 0.05. *, P < 0.05; **, P < 0.01.

in astrocytes. It was revealed that, similar to the transcriptomic changes observed in the bulk tissue of spinal cord (Fig. 3 B), expression of differentially expressed genes associated with NF-κB signaling and immune response was also significantly reduced in astrocytes between genotypes (Fig. 3 E). KEGG analysis showed that 14 out of top 30 listed pathways were related to infection, immune responses, phagosome, and lysosome (Fig. 3 F). Moreover, Gene Ontology (GO) enrichment of the differentially expressed genes between the genotypes revealed that the most significant biological processes were related to purinergic nucleotide receptor/adenosine receptor signaling pathway (e.g., *P2ry1*, *P2ry12*, *Adora2a*), IL-18 production (e.g., *Nlrp3*, *Tlr9*), and negative regulation of IL-1β secretion (e.g., *Gas6*, *Nlrp3*), confirming the key role for DRD2 in the regulation of astrocyte-driven inflammation. Together, these data suggest that selective deficiency of aDRD2 is required for the suppression of inflammatory response and neuronal survival in EAE, supporting the idea that activation of DRD2 signaling in whiter matter astrocytes may be detrimental to the CNS.

As shown in Fig. 3, B and E, NF-κB pathway was remarkably deactivated in *Drd2* cKO EAE mice. To validate these findings, we evaluated the impact of altering DRD2 expression in astrocytes on inflammatory response. Loss of *Drd2* led to a marked reduction in levels of several NF-κB–signaling proteins and cytokines, such as IκBα, p65, IL-1β, and TNF-α, at the peak of the disease when compared to control (Fig. 3, G and H). In contrast, mice lacking *Drd2* selectively in neurons displayed no significant alteration in levels of proinflammatory mediators in the spinal cord in vivo (Fig. 3 I), confirming that control of CNS inflammatory response in EAE is heavily dependent on DRD2 in astrocytes, but not in neurons (Fig. 2).

DRD2 controls the expression of PTS

To explore the molecular mechanisms that are responsible for regulating aDRD2 signaling in EAE, we searched for the candidate genes by analyzing RNA-seq and DNA microarray data (Fig. 3, A and D). The suitable candidate genes were selected based on whether its expression is dependent on DRD2 and its association with EAE course. GO enrichment of the differentially expressed genes in astrocytes between the genotypes in DNA microarray data (Fig. 3 E) showed that among the top-ranked biological processes in astrocytes, the tetrahydrobiopterin (BH4) biosynthetic process (e.g., *PTS*, *Pcbd1*, *Pcbd2*) was also indicated. Interestingly, analysis of the gene transcription expression profiles of the spinal cord tissue of *Drd2* cKO EAE mice also revealed that *PTS* showed the greatest reduction among the most differentially expressed genes between genotypes under both basal condition and EAE induction (Figs. 3 A and 4 A). PTS is one of the enzymes responsible for the biosynthesis of BH4, which is an essential cofactor for tyrosine hydroxylase and tryptophan hydroxylase as well as for phenylalanine hydroxylase in the process of DA and serotonin biosynthesis (Laufs et al., 1998). Whether PTS plays a role in neuroinflammation has not yet been explored.

To unravel the role of PTS in the pathogenesis of EAE, we first assessed PTS expression in mice. We found that PTS was abundantly expressed in astrocytes and neuronal cells, but at low levels in microglia and NG2 glia under basal condition, as revealed by immunohistochemical staining (Fig. 4 B). There was a marked decrease in PTS expression levels in astrocytes in *Drd2*^{mGFAP} mice, which showed a great amelioration in EAE phenotype (Fig. 2 A), following EAE induction as compared with their wild-type littermates on the peak of the disease, suggesting that the activation of astrocytes was dramatically reduced. This was supported by the observations that the intensities of GFAP immunosignals were profoundly decreased (Fig. 4, C and D), indicating a positive correlation between activation of PTS-expressing astrocytes and EAE phenotype.

Upregulation of PTS in MS brain

To determine the clinical relevance of PTS expression with MS, we examined the expression of PTS in the brain of patients with MS using immunostaining. In agreement with the observations in mouse brain shown in Fig. 4 B, there was a strong enhancement in the density of PTS immunosignals in the white matter surrounding the MS lesion sites, most of which were confined to astrocytes compared to the normal white matter (Fig. 4, E and F). Notably, there were no PTS^{+} cells showing intact cell morphology within the active lesion sites, indicating poor survival of these cells (data not shown). We also found colocalization of PTS with neuronal marker NeuN, suggesting expression of PTS in neurons (Fig. 4 G). In contrast, microglia were not immunoreactive for PTS (Fig. 4 G). Together, these data indicate that astrocytic PTS signaling in astrocytes is associated with neuroinflammation in MS.

PTS promotes CNS inflammation

Next, we evaluated the functional impact of astrocytic PTS on EAE phenotype in vivo. Knockdown of *PTS* was achieved by lentivirus (LV)-mediated shRNA targeting PTS that was under the control of GFABC1D promoter (Lee et al., 2008; Fig. 5 A). Wild-type mice received a single intracerebroventricular

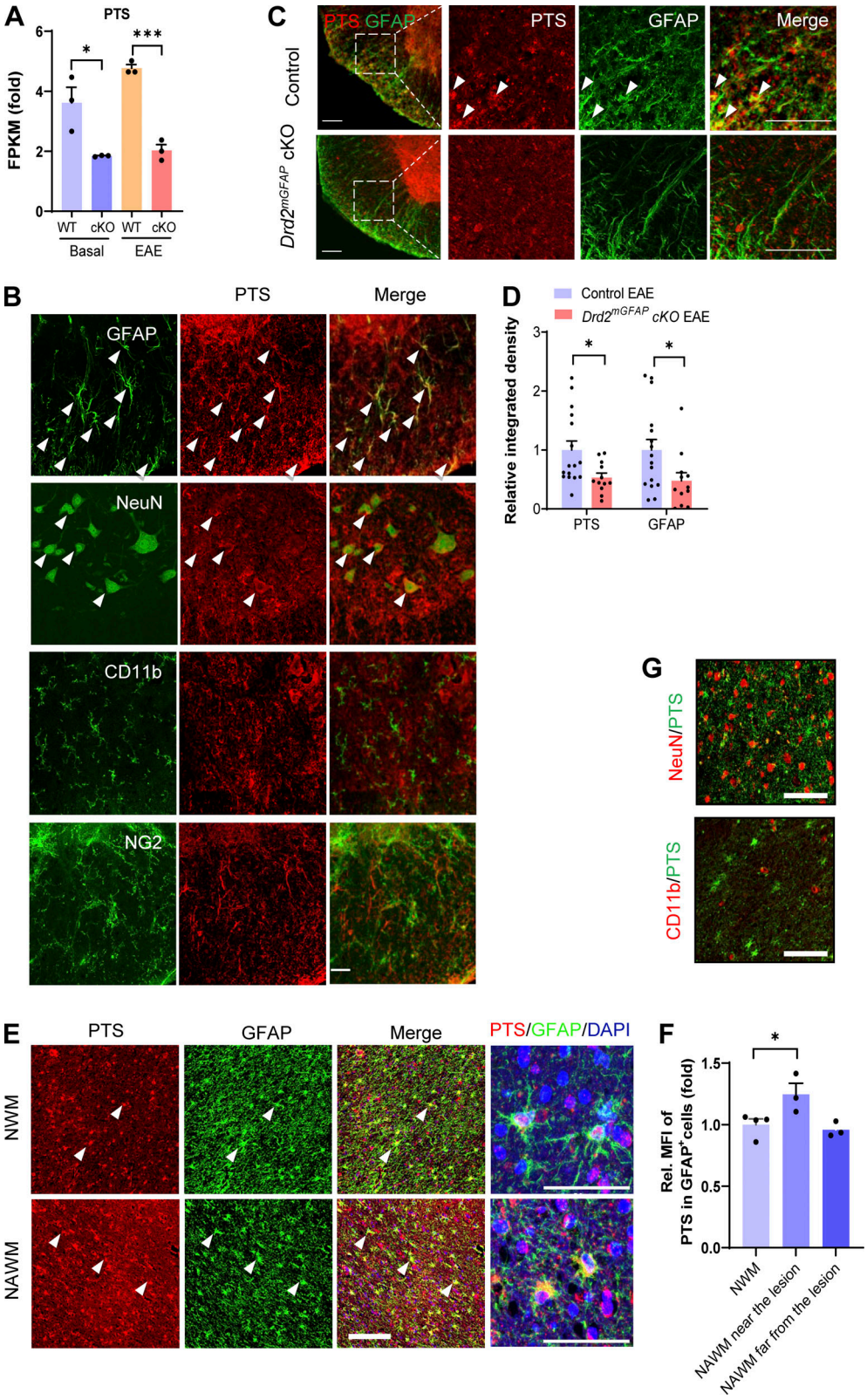

Figure 4. **Expression of astrocytic PTS is controlled by DRD2 and is upregulated in the brain of patients with MS. (A)** The FPKM values of PTS gene in the spinal cord tissue of *Drd2*^{mGFAP} cKO and control mice on day 17 after EAE induction revealed by RNA-seq analysis, as shown in Fig. 3. *n* = 3 mice per group. **(B)** Immunofluorescent histochemical staining for PTS, GFAP, IBA1, and NG2 on the spinal cord of 2-mo-old wild-type mice. Scale bar, 50 mm. The arrowheads point to the cells with co-expression of PTS and GFAP. **(C and D)** Immunofluorescent histochemical staining for PTS and GFAP on the spinal cord of *Drd2*^{mGFAP} cKO and control mice on day 17 after EAE induction (C) and quantitative data (D). *n* = 4 mice per group. The arrowheads point to the cells with co-expression of PTS and GFAP. Scale bars, 100 mm. **(E and F)** Representative immunofluorescent microphotographs showing PTS$^+$ astrocytes in the white matter of brain from

patients with MS (n = 3) and control individuals (n = 3). The arrowheads point to the cells with co-expression of PTS and GFAP. Quantitative data of E are shown in F. Scale bars, 200 mm. **(G)** Representative immunofluorescent microphotographs showing expression of PTS, NeuN, and CD11b in MS brain. Scale bar, 100 mm. NWM, normal white matter; NAWM, normally appearing white matter. Data are represented as mean ± SEM. P values are from unpaired t tests, in which ns (not significant) indicates P > 0.05. *, P < 0.05; ***, P < 0.001.

injection of LV vector 3~7 d before EAE induction. Selective *PTS* deficiency in astrocytes resulted in a remarkable attenuation in disease severity of EAE, showing a robust delay in the onset of EAE and a dramatic reduction in the EAE severity (Fig. 5 B), which resembles EAE-challenged *Drd2*^{mGFAP} cKO mice shown in Fig. 2 A. The animals with clinical symptoms relieved displayed ameliorated inflammatory responses, by showing reduced activation of astrocytes, but not microglia (Fig. 5, C and D), concomitant with downregulation of proinflammatory mediators, as well as NF-κB pathway signaling proteins in the spinal cord on the peak of the disease as compared with the controls (Fig. 5, E–G).

The NF-κB pathway is known to play a key role in immunity and inflammation (Hayden and Ghosh, 2012; Mattson and Camandola, 2001; van Loo et al., 2006). To further determine the causal relationship between DRD2/PTS axis and NF-κB signaling, we constructed a human embryo kidney (HEK)–293T cell line stably expressing the NF-κB luciferase reporter gene, under the control of multimerized NF-κB responsive element upstream of a minimal promoter (Pessara and Koch, 1990; Baeuerle, 1998; Fig. S5 A). We found that overexpression of either PTS or DRD2 in HEK293T cells expressing NF-κB luciferase reporter gene profoundly promoted NF-κB luciferase activities compared to control. This increased activity was further elevated upon TNF-α stimulation, as compared to PTS or DRD2 overexpression alone (Fig. 5, H and I; and Fig. S5 B), indicating a synergistic effect between DRD2/PTS axis and TNF receptor signaling on NF-κB activation. Interestingly, knockdown of PTS remarkably suppressed DRD2 overexpression-induced augmentation in NF-κB luciferase activities, indicating that PTS mediates DRD2-induced activation of astrocytes (Fig. 5 I). Together, these data suggest that astrocytic PTS is a key modulator of neuroinflammation in EAE.

Protein kinase C-δ (PKCδ) activation mediates DRD2/PTS axis–promoted inflammation

Next, we investigated the regulatory mechanisms underlying DRD2/PTS axis–promoted neuroinflammation. Given that aDRD2-modulated inflammatory response is associated with NF-κB signaling (Fig. 3) and there is a remarkable resemblance in the mitigation of EAE phenotype between *PTS*-knockdown mice and *Drd2* cKO mice (Figs. 3 and 5), we thus speculated that DRD2/PTS axis may activate NF-κB pathway in astrocytes during inflammation. To test this, coimmunoprecipitation assay was employed to examine whether PTS interacts with a NF-κB–signaling protein(s). It was revealed that PTS did not interact with major NF-κB–signaling proteins tested, such as PKCδ, TAK1, TRAF6, IκBa, and p65 (data not shown). Interestingly, PTS bound to the cleaved form of PKCδ in HEK293T cells (Fig. 6, A and B). PKCδ is known to be associated with the activation of NF-κB leading to microglia activation (Burguillos et al., 2011; Kavanagh et al., 2014). Activation of PKCδ promoted NF-κB activity via IKK (Spiegel and Milstien, 2011). Our result indicates that PTS may stabilize the active form of PKCδ via their binding activity, leading to prolonged or stronger activation of PKCδ/NF-κB signaling. This was supported by the observations that PTS-induced elevation in NF-κB activity was significantly inhibited by PKCδ inhibitor Rottlerin in a dose-dependent manner, as assessed by NF-κB luciferase reporter assay (Fig. 6 C). These results suggest that PKCδ activation is required for PTS-induced NF-κB activation.

We found that, similar to the effect of PTS, DRD2 overexpression also led to increased activation of PKCδ which was further markedly augmented following exposure to TNF-α, as there were profound increases in protein levels of cleaved PKCδ in TNF-α–treated HEK293T cells (Fig. 6, D and E). Consistent with data shown in Fig. 5 I, the results of pharmacological treatment confirmed that PKCδ activation mediated DRD2-induced inflammation, as blockade of PKCδ with Rottlerin resulted in a pronounced inhibition of NF-κB activities in a dose-dependent manner (Fig. 6 F). Furthermore, DRD2-induced NF-κB activation can be abrogated by IKKα/β inhibitor PS1145 (Fig. 6 G). Together, these data suggest that PKCδ plays a key role in regulating the proinflammatory response driven by astrocytic DRD2/PTS axis.

DA/DRD2 signaling alters NF-κB activation

Next, we sought to determine whether aDRD2 responds to the neurotransmitter DA during inflammation. Treatment of HEK293T cells stably overexpressing DRD2 and NF-κB luciferase reporter gene with DA induced stronger NF-κB activation, which was augmented by TNF-α (Fig. S5 C). Consistent with this result, cabergoline, a potent DRD2 agonist commonly used in Parkinson's disease treatment, showed a similar effect (Fig. S5 C). Notably, other commonly used agonists known targeting neuronal DRD2, such as quinpirole and phenethylamine, failed to induce inflammatory response (Fig. S5 C). These results suggest that aDRD2 has a different functional characteristic from neuronal one in the modulation of NF-κB signaling.

Dehydrocorybulbine (DHCB) inhibits aDRD2/PTS/PKCδ signaling

To search for a potential aDRD2 antagonist that also exerts an anti-inflammatory activity, a variety of clinically approved and investigational drugs that target DRD2 were screened by using NF-κB luciferase reporter assay. We found that among them, DRD2 antagonists DHCB (Zhang et al., 2014) and L-741,626 (Hill et al., 2006) showed significant inhibitory activities on DRD2/TNF-α–induced elevation of NF-κB activity (Fig. S5 C). In contrast, other classical DRD2 antagonists tested, such as haloperidol and nemonapride, failed to show the same effects (Fig. S5 C), confirming that aDRD2 has a distinct property from neuronal one.

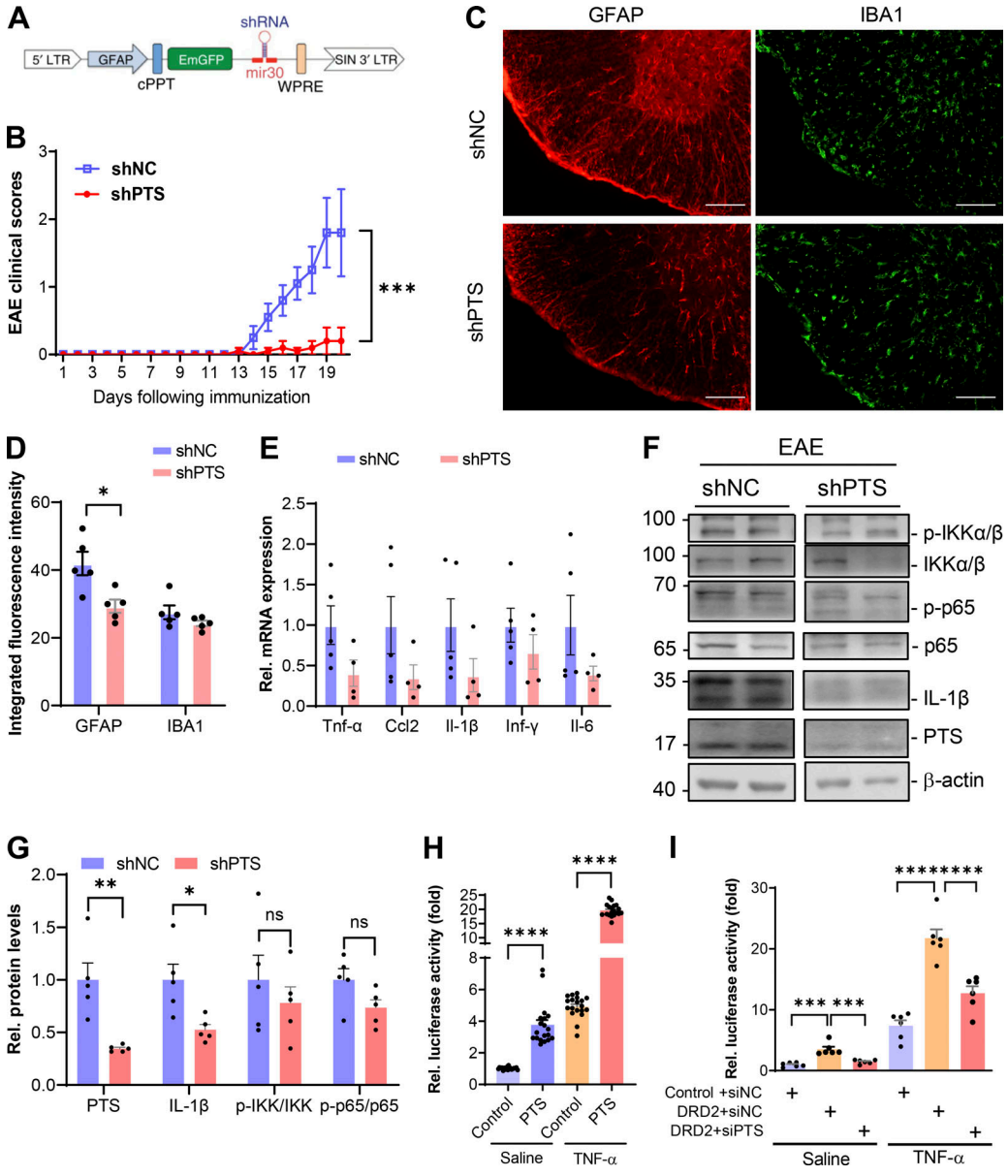

Figure 5. **Selective *PTS* deficiency in astrocytes attenuates EAE. (A)** Schematic diagram showing the LV construct used for astrocyte-specific PTS knockdown. WPRE, woodchuck posttranscriptional regulatory element; cPPT, central polypurine tract. **(B)** Representative graph showing average clinical scores of wild-type mice received intracerebroventricular injection of LV-GFABC1D-shPTS and control construct. *n* = 10 per group. **(C and D)** Immunofluorescent histochemical staining for GFAP and Iba1 on the spinal cord of wild-type mice received intracerebroventricular injection of LV-GFABC1D-shPTS on day 20 after EAE induction (C) and quantitative data (D). Scale bars, 100 µm. *n* = 5 mice per group. NC, negative control. **(E)** Representative graph showing relative mRNA levels of inflammatory mediators in the spinal cord of wild-type mice injected with LV-GFABC1D-shPTS and control construct (*n* = 5). **(F and G)** Immunoblot analysis of tissue lysates from wild-type mice received intracerebroventricular injection of LV-GFABC1D-shPTS on day 20 after EAE induction (F) and quantitative data (G). *n* = 5 mice per group. **(H)** Representative graph showing NF-κB luciferase activities in HEK293T cells coexpressing PTS and NF-κB luciferase reporter gene in the presence of TNF-α or vehicle. *n* = 6. **(I)** Representative graph showing NF-κB luciferase activities in HEK293T cells coexpressing DRD2, siPTS, and NF-κB luciferase reporter gene in the presence of TNF-α or vehicle. Experiments are repeated at least three times in triplicates. Data are represented as mean ± SEM. P values are from unpaired *t* tests (D and G–I) or two-way ANOVA (B), in which ns (not significant) indicates P > 0.05. *, P < 0.05; **, P < 0.01; ***, P < 0.001; ****, P < 0.0001.

DHCB, isolated from the traditional Chinese medicine *Corydalis yanhusuo* W. T. Wang, is shown to be able to penetrate the blood-brain barrier and function as a novel analgesic with moderate DRD2 antagonist activities (Zhang et al., 2014). Next, we sought to determine the influence of DHCB on the DRD2 signaling. Coimmunoprecipitation analysis showed that exposure to DHCB reduced the binding between PTS and the cleaved form of PKCδ (Fig. 7 A). Consequently, it caused a marked attenuation of DRD2/TNF-α–induced PKCδ activation (Fig. 7, B and C), suggesting an inhibitory effect of DHCB on the activation of NF-κB pathway. In accordance with these data, activation of NF-κB pathway provoked by TNF-α and

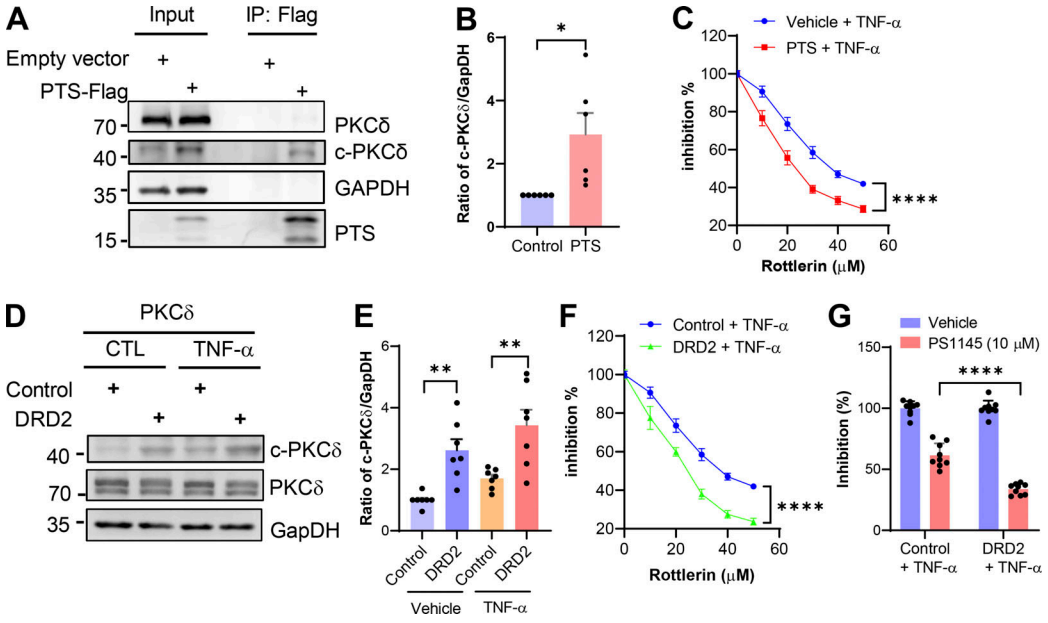

Figure 6. **Activation of astrocytic DRD2 promotes inflammatory response via the activation of PKCδ with is regulated by PTS. (A and B)** Representative immunoblots of coimmunoprecipitation assay showing the binding between PTS and the cleaved form of PKCδ in HEK293T cells (A) and quantitative data (B). *n* = 5. **(C)** Pharmacological blockade of PKCδ with Rottlerin inhibits NF-κB activity induced by PTS in combination with TNF-α in HEK293T cells, revealed by NF-κB luciferase assay. *n* = 3. **(D and E)** Representative immunoblots showing DRD2-induces the cleavage of PKCδ (cPKCδ) in HEK293T cells overexpressing DRD2 and PKCδ, or in combination with exposure to TNF-α (D) and quantitative data (E). *n* = 3. **(F)** NF-κB luciferase assay showing effect of pharmacological blockade of PKCδ with Rottlerin on NF-κB activity of HEK293T cells expressing DRD2. *n* = 3. **(G)** NF-κB luciferase assay showing effect of pharmacological blockade of IKKα/β with PS1145 on NF-κB activity of HEK293T cells expressing DRD2. Data are represented as mean ± SEM. P values are from unpaired *t* tests (B, E, and G) or two-way ANOVA (C and F). *, P < 0.05; **, P < 0.01; ****, P < 0.0001.

endogenous DRD2 was profoundly reduced by DHCB, as evidenced by inhibition of phosphorylation of NF-κB–signaling proteins (Fig. 7, D and E), which occurred concurrently with a profound reduction in the production of proinflammatory mediator iNOS (Fig. 7, F and G).

To investigate the impact of the two selected DRD2 antagonists DHCB and L-741,626 on the EAE course in vivo, mice lacking neuronal *Drd2* (*Drd2*^{Thy1} cKO) mice were administered with either compound throughout the course of EAE. The use of *Drd2*^{Thy1} cKO mice allowed for better assessment of DHCB on glial DRD2 with relatively higher cell-type specificity, given that DHCB may have antagonistic activity on DRD2 in multiple cell types, including neuronal DRD2 (Zhang et al., 2014). Repeated administration of DHCB resulted in a remarkable reduction in EAE severity in *Drd2*^{Thy1} cKO mice, as compared to control (Fig. 7 H), which was accompanied by robustly attenuated progression of demyelination and mitigated monocytes infiltration into the spinal cord in EAE (Fig. 7 I). Moreover, there was a marked reduction in the activation of NF-κB pathway and the production of proinflammatory mediator pro–IL-1β in animals administered with DHCB, as evidenced by downregulated phosphorylation of multiple NF-κB signaling phosphoproteins, detected by immunoblotting (Fig. 7, J and K). In contrast, treatment of global *Drd2* KO mice with DHCB did not significantly alter EAE disease severity as compared to vehicle-treated *Drd2* KO mice (Fig. 7 L), indicating that DHCB does not have non-DRD2 effect on EAE. Furthermore, administration of L-741,626 did not significantly ameliorate the clinical symptom of EAE (Fig. 7 M), indicating that aDRD2 possesses different property from neuronal one which is targeted by conventional DRD2 antagonists. This notion was supported by the observations that wild-type mice, which were administered with either the combination of DRD2 antagonists (haloperidol and spiperone) or the combination of DRD2 agonists (quinpirole and rotigotine) before and throughout the course of EAE, exhibited no significant alteration in the clinical performance of EAE (Fig. 7 N). These results were consistent with the in vitro data shown in Fig. S5, thus confirming that conventional DRD2 agonists or antagonists have little or no influence on EAE course via modulating DRD2 activity. Taken together, these data suggest that blockade of aDRD2 with DHCB abrogates neuroinflammation and neurodegeneration in EAE.

Discussion

Despite the increasing appreciation of the importance of CNS glial cells under pathological conditions, including EAE and MS, the molecular and cellular mechanisms underlying the regulation of astrocyte-associated CNS innate immunity and the functional contribution of these mechanisms to the EAE/MS pathogenesis remain elusive. In the present study, we identify DRD2 in astrocytes, but not in neurons, as a determinant of white matter astrocyte activation leading to the sustained inflammation primarily within the CNS during EAE. We found that selective ablation of *aDrd2* remarkably abrogated EAE progression. Moreover, *aDrd2* tightly controlled the expression

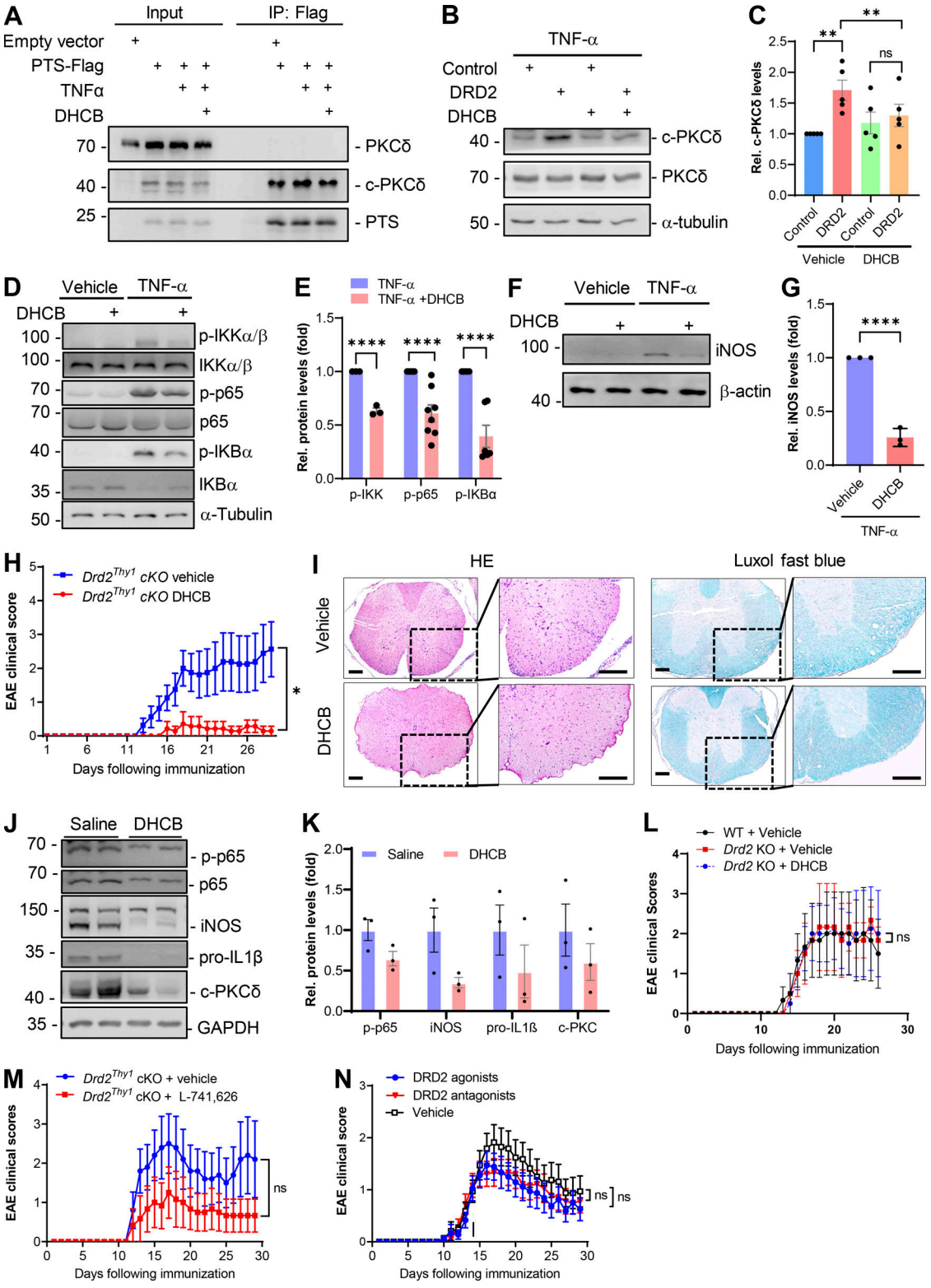

Figure 7. **Blockade of astrocytic DRD2 with DHCB attenuates inflammatory response and mitigates EAE severity. (A)** Coimmunoprecipitation assay showing the interaction between PTS and PKCδ in HEK293T cells. HEK293T were stimulated by DHCB (100 μM) for 30 min and TNF-α (20 ng/ml) for 6 h. **(B and C)** Representative immunoblots showing levels of cleaved PKCδ and corresponding noncleaved forms in DHCB-treated 293T cells overexpressing PKCδ, and DRD2 in the presence of TNF-α (B) and quantitative data (C). **(D and E)** Representative immunoblots showing levels of phospho-IKKα/β, phospho-IκBα, phospho-p65, and their corresponding nonphosphorylated forms in DHCB-treated primary cultured astrocytes (D) and quantitative data (E). *n* = 3. **(F and G)** Representative immunoblots showing iNOS levels in primary cultured astrocytes exposed to DHCB (F) and quantitative data (G). *n* = 3. **(H)** Representative graph showing average clinical scores of *Drd2*^{Thy1} cKO mice treated with DHCB (20 mg/kg, i.p., daily) or vehicle. *n* = 9 for DHCB, *n* = 8 for vehicle. **(I)** Representative Luxol fast blue and hematoxylin and eosin (HE) staining on the spinal cord sections of *Drd2*^{Thy1} cKO mice and control administered with DHCB are

shown. The animals are sacrificed on day 17 after EAE induction. Scale bars, 100 mm. **(J and K)** Immunoblot analysis of tissue lysates from *Drd2*^{Thy1} cKO mice administered with DHCB and control on day 17 after EAE induction (J) and quantitative data (K). p-p65: P = 0.088; iNOS: P = 0.081. *n* = 3. **(L)** Representative graph showing average clinical scores of *Drd2* KO mice administered with DHCB. WT + Vehicle, *n* = 3; *Drd2* KO + Vehicle, *n* = 3; *Drd2* KO + DHCB, *n* = 4. **(M)** Representative graph showing average clinical scores of wild-type mice administered with L-741,626. Vehicle, *n* = 5; L-741,626, *n* = 6. **(N)** Representative graph showing average clinical scores of age-matched wild-type mice administered with either combination of DRD2 agonists (quinpirole and rotigotine, *n* = 18 mice) or antagonists (haloperidol and spiperone, *n* = 18 mice) or vehicle (*n* = 17 mice). Data are represented as mean ± SEM. P values are from unpaired *t* tests (E, G, and K) or two-way ANOVA (C, H, L, and M), in which ns (not significant) indicates P > 0.05. *, P < 0.05; **, P < 0.01; and ****, P < 0.0001.

of PTS, which robustly regulates NF-κB pathway–dependent inflammatory response via PKCδ. Treatment of either DA or DRD2 agonist cabergoline activated NF-κB pathway. Blockade of aDRD2 signaling using DHCB remarkably attenuated EAE phenotype. Our data suggest that DRD2/PTS/PKCδ signaling in astrocytes plays a key role in the propagation of inflammatory response that is a critical machinery driving neurodegeneration in EAE.

Astrocytes in the CNS have long been viewed as secondary participators to insults in MS and passive recipients of outcomes, by forming astroglial scar and producing cytokines (Brosnan and Raine, 2013). In contrast, we found here that astrocyte-regulated CNS innate immunity plays a key role in the control of EAE progression, as mice lacking *Drd2* in astrocytes displayed a dramatic decrease of inflammatory response selectively in the CNS in EAE, suggesting that among CNS glial cells, such as microglia and oligodendrocytes, astrocytes play a leading role in EAE pathogenesis. This notion is supported by our finding that silence of astrocytes by *Drd2* deletion is sufficient to diminish neuroinflammation, despite robust inflammatory response in the peripheral immune system. This phenomenon is consistent with previous studies showing that there is altered DNA methylation in CNS-resident cells of patients with MS but not in peripheral immune cells (Huynh et al., 2014; Baranzini et al., 2010). Thus, our data confirm that DRD2-mediated astrocyte activation is crucial for determining disease outcomes in EAE.

Insights into aDRD2 control of proinflammatory response

There are several plausible mechanisms by which DRD2/PTS/PKCδ signaling-regulated astrocytes could contribute to autoimmunity and neurodegeneration. Astrocytes have direct neurodegenerative functions mediated by the DRD2/PTS/PKCδ axis–controlled production of cytokines, such as TNF-α and IL-1β. Moreover, mice lacking *Drd2* in astrocytes or *PTS*-deficient astrocytes displayed a marked reduction in levels of cytokines and chemokines and a remarkable decrease in numbers of peripheral lymphocytes infiltrated into the CNS, suggesting that astrocyte activation facilitated by DRD2/PTS/PKCδ axis is required for immune cell extravasation into the CNS during EAE. The activated astrocytes also robustly influence the activity of innate immune cells, including microglia and infiltrated monocytes in the CNS (Fig. S3), thereby promoting neurodegeneration. Indeed, neurodegeneration in MOG_{35-55}-induced EAE is almost diminished following depletion of *aDrd2* (Fig. 2), implying that astrocytes are at the interface between the CNS and immune system, being capable of integrating a variety of incoming signals and directing the downstream inflammatory response. Together, these actions represent new mechanisms by which astrocytes mediate CNS inflammation in EAE.

There is increasing evidence that receptors expressed on the CNS-resident immune cells serve as potential sensors of molecules that induce or amplify inflammatory signals in neurodegenerative diseases (Wang et al., 2015; Yang and Zhou, 2019). It has been believed that astrocytes are able to sense and propagate immunosignals such as TNF-α, released from microglia in neuroinflammation, as a part of secondary immune response via a variety of receptors (Glass et al., 2010). Whether astrocytes respond to other stimuli except for cytokines remain incompletely understood. We found that DA provokes NF-κB activity and selective deficiency of *Drd2* in astrocytes diminishes inflammatory responses in EAE. DA also jointly functions with proinflammatory mediators, such as TNF-α, to synergistically amplify inflammation. These findings indicate that DA participates in inflammation via aDRD2 as a costimulatory molecule. This effect is opposite to that in peripheral immune system seen by others, where DRD2 along with DRD3–5 are generally considered to be anti-inflammatory (Melnikov et al., 2020; Wu et al., 2020). Thus, aDRD2 signaling represents a distinct pathological role of DA in the CNS during EAE. It is worthy to mention that actively induced EAE depends on a profound and global inflammatory response triggered by the adjuvants. It is likely that CFA alone induces global inflammatory response that may well affect glial cell response. Whether EAE induced in the absence of CFA is also regulated by aDRD2 needs to be investigated in future.

We showed the significant effect of DA on the activation of NF-κB pathway, which can be mimicked by DRD2 agonist cabergoline (Fig. S5 C). This detrimental effect of DA during EAE is consistent with a recent finding that neurotransmitter norepinephrine mediated colon inflammation in mouse colons during acute dextran sulfate sodium–induced colitis (Sun et al., 2021), demonstrating a previously unrecognized detrimental role of catecholamines. In the context of EAE, DA that influences astrocytes may originate from several sources, including activated immune cells that invade the CNS and DAergic innervation in the spinal cord (Lindvall et al., 1983), as well as the influx of the plasma which contain DA due to the BBB leakage. Indeed, multiple studies have shown diffuse and extensive BBB disruption in MS and EAE model, which correlates with the sites of inflammatory cell accumulation (Grossman et al., 1986; Paty and McFarland, 1998; Badawi et al., 2012). The BBB disruption appears to parallel disease progression in MS (Bennett et al., 2010; Wojkowska et al., 2014). It is likely that DA derived from these potential sources act jointly to influence the microenvironment at the point of inflammation during the process of neurodegeneration.

The effect of aDRD2 in mouse models of different CNS diseases is complex, with both pathological and protective roles identified. Previous studies have shown that the deficiency of

aDrd2 contributes to increased vulnerability of nigral dopaminergic neurons to neurotoxin-induced neurotoxicity in a Parkinson's disease animal model, by producing glial scar in the gray matter and proinflammatory mediators (Shao et al., 2013; Zhu et al., 2018). Somewhat surprisingly, these findings are opposite to the observations in the present study. This discrepancy may be associated with whether the axons are myelinated. It is known that DAergic neurons have highly branched and unmyelinated fibers (Surmeier, 2018). The discrepancy is also attributable to the heterogeneity in astrocyte subpopulations between the white matter and gray matter, and the distinct nature of insults and inflammatory processes. These factors are likely determinants of specific pathological processes of MS and Parkinson's disease, implying that cell type–specific blockade of DRD2 is required for the intervention of individual brain diseases.

Astrocyte-specific effects on DRD2 modulation are likely attributable to the fact that there are profound differences between neuronal DRD2 and astrocytic one. There is a unique post-translational modification in aDRD2 compared with neuronal one. Moreover, concerning intracellular signaling, aDRD2 links to PTS, a downstream protein of DRD2, mediating the modulation of inflammation, whereas in neuronal cells, PTS is known to be involved in the biosynthesis of BH4 (Linscheid et al., 1998; Franscini et al., 2003), but with no profound influence on neuroinflammation. Therefore, a specific antagonist targeting aDRD2 that modulates neuroinflammation, but with no blocking activity on neuronal DRD2, is desirable. Currently, most of the classical DRD2 antagonists primarily have blocking activity on neuronal DRD2. In the present study, as a first step forward, DHCB is identified as a compound that targets both neuronal and aDRD2. A highly selective aDRD2 antagonist without causing the side effects through neuronal DRD2 needs to be identified in future studies. In summary, the present study reveals previously uncharted mechanisms of disease pathogenesis and raises the possibility that blockade of DRD2/PTS signaling in astrocytes could provide therapeutic benefit in autoimmunity diseases such as MS.

Materials and methods

Human tissue collection

Fresh-frozen cerebral brain tissues and tissue sections were obtained from the Netherlands Brain Bank, Netherlands Institute for Neuroscience, Amsterdam, Netherlands. All the materials have been collected from donors for or from whom a written informed consent for a brain autopsy and the use of the material and clinical information for research purposes had been obtained by the Netherlands Brain Bank. For immunoblot analyses, frozen brain tissues from seven pairs of age, gender, postmortem interval-matched MS patients, and nondemented controls were used. For immunofluorescent staining, paraffin sections from four pairs of age, gender, post-mortem interval-matched MS patients, and normal-appearing white matter of controls were used. All the MS subjects were clinically and neuropathologically diagnosed, and the healthy control subjects were described previously by Hendrickx et al. (2017). This study was reviewed and approved by the Institutional Bioethics Committee, Institute of Neuroscience, Chinese Academy of Sciences, China, under ethical approval number ION-2017-001.

Animals

Adult or neonatal C57BL/6 mice were from Shanghai Laboratory Animal Center, Chinese Academy of Sciences. Two global *Drd2* KO mouse lines were used: mouse line number 1 was provided by Dr. Z.L. Huang (Yamaguchi et al., 1996) and mouse line number 2 (*B6.129S2-Drd2*^{tm1Low}*/J*) was from The Jackson Laboratory. *Drd2*-floxed mice were created by Shanghai Research Center for Model Organisms (Shanghai, China; Shao et al., 2013). Briefly, the floxed *Drd2* allele was generated by introduction of loxP sites flanking the first coding exon (exon 2) of the *Drd2* locus into the mouse genome. Recombinant embryonic stem cells were injected into C57BL/6 blastocysts to produce chimeras which were then crossed to C57BL/6 mice to produce mice heterozygous for the floxed *Drd2* allele (*Drd2*$^{flox/+}$; Shao et al., 2013) for at least ten generations before use. Mouse GFAP (mGFAP)-Cre transgenic mice (*B6.Cg-Tg(Gfap-cre)*$^{77.6Mvs}$*/2J*, #024098; JAX stock; Gregorian et al., 2009), thymocyte antigen 1 promoter transgenic mice (*FVB/N-Tg(Thy1-cre)1*^{Vln}*/J*, #006143; JAX stock) was purchased from The Jackson Laboratory. Those strains that were originally not in a C57BL/6 (inbred) genetic background were backcrossed for ten generations prior to use. Characterization and genotyping of these mice were described previously (Cai et al., 2011). They were maintained on a 12-h light/dark cycle at 23°C with food and water available ad libitum. Animal maintenance and handling were approved by the Institutional Animal Care and Use Committee (IACUC no. NA-004-2016) and were in accordance with the U.S. National Institutes of Health *Guide for the Care and Use of Laboratory Animals*.

Randomization and blinding

No specific randomization was used. Experiments were performed in a collaborative manner among multiple members of the team, which makes single-blind experiments feasible. For example, experimenters were blinded to genotype during EAE scoring.

Western blot analysis and quantification

Western blotting was performed as described previously (Li et al., 2006). The following primary antibodies were used: (a) mouse anti-GFAP mAb (1:1,000; G3893; Sigma-Aldrich); (b) rabbit anti-GFAP pAb (1:2,000; Z0334; DAKO); (c) rabbit anti-IBA1 pAb (1:1,000; 019-19741; WAKO); (d) rabbit anti–IL-1β pAb (1:1,000; sc7884; Santa Cruz); (e) rabbit anti–p-IKBα (Ser32/Ser36) pAb (1:1,000; 9246; Cell Signaling Technology); (f) rabbit anti-IKBα pAb (1:1,000; 5242; Cell Signaling Technology); (g) rabbit anti–NF-κB (p65) pAb (1:1,000; sc-109; Santa Cruz); (h) rabbit anti–p-NF-κB (p-p65) pAb (1:1,000; 3033; Cell Signaling Technology); (i) rabbit anti-PKCδ mAb (1: 1,000; ab182126; Abcam); (j) rabbit anti-PTS pAb (1:1,000; STJ28228; St John's Laboratory); (k) mouse anti-iNOS mAb (1:1,000; 610431; BD Transduction Laboratories); (l) mouse anti-GAPDH mAb (1: 5,000; 1336; SAB); (m) mouse anti–β-actin mAb (1:5,000; A5441; Sigma-Aldrich); (n) guinea pig anti-NeuN (1:1,000, ABN90;

Millipore); (o) mouse anti–α-tubulin (1:5,000; T6199; Sigma-Aldrich); (p) rabbit anti-DRD2 (1:1,000, AB_2571596; Frontier Institute Co. Ltd); (q) rabbit anti–TNF-α (1:1,000, ab6671; Abcam); (r) rabbit anti-IKK a/b (1:1,000; sc-7607; Santa Cruz); (s) rabbit anti–p-IKKα/β (1:1,000; 2697; Cell signaling Technology). The membrane was washed and incubated for 1 h at room temperature with the corresponding secondary antibodies: (a) HRP-conjugated goat antirabbit IgG (1:10,000; Jackson ImmunoResearch Laboratories) and (b) HRP-conjugated goat antimouse IgG (1:10,000; Jackson ImmunoResearch Laboratories). Peroxidase activity was detected with SuperSignal WestPico chemiluminescent substrate (Pierce Biotechnology) and visualized and digitized with ImageQuant (LAS-4000; Fujifilm). Optical densities of bands were analyzed by ImageJ (version 1.49k, National Institutes of Health).

Immunofluorescence, confocal microscopy, and image analysis

Spinal cord cryo-sections were incubated with one primary antibody followed by incubation with another primary antibody. The same sections were then incubated with the appropriate secondary antibodies. For formalin-fixed, paraffin-embedded tissue specimens, they were sectioned in the thickness of 5 µm followed by deparaffinized and incubation with 0.01 M sodium citrate (pH 6.0) at 100°C for 15 min to retrieve antigens. The sections were then treated with 0.5% (wt/vol in 70% alcohol) Sudan black at 37°C for 40 min to eliminate nonspecific fluorescence before immunofluorescence staining. Sections were imaged using either laser confocal microscope (Nikon A1 or A1R) or a BX51 microscope (Olympus). Data were obtained and processed using ImageJ. Relative-integrated densities of PTS, GFAP, or IBA1-immunopositive regions in the white matter of mouse spinal cord were calculated using ImageJ, in 20× images taken from three to seven sections. Mean-integrated density values are reported as mean gray value × percentages of area above background ± SEM.

Immunofluorescent histochemical analysis of human brain sections was performed as previously described (Rothhammer et al., 2018). The brain sections were deparaffinized and the antigens were retrieved. Further staining steps were carried out with the 4-plex IHC staining kit (WiSee Biotechnol) according to the manufacturer's instructions. The relative integrated density in six to nine fields per sample under 20 × from three to four MS brain and three to four control subjects was measured.

The following primary antibodies were used: (a) mouse anti-GFAP mAb (1:1,000; Sigma-Aldrich); (b) rabbit anti-GFAP pAb (1:2,000; DAKO); (c) rabbit anti-IBA1 pAb (1:1,000; WAKO); (d) guinea pig anti-NeuN pAb (1:500; Millipore); (e) mouse anti-MBP mAb (1:500; Calbiochem); (f) rabbit anti-PTS pAb (1:500; GeneTex); and (g) rabbit anti-DRD2 (1:100, AB_2571596; Frontier Institute Co. Ltd).

The following secondary antibodies were used: Alexa Fluor 555 goat antimouse IgG (A-21422; Invitrogen); Alexa Fluor 488 goat antimouse IgG (A-11001; Invitrogen); Alexa Fluor 488 goat antirabbit IgG (A27034; Invitrogen); Alexa Fluor 647 goat antimouse IgG (A-21235; Invitrogen); Alexa Fluor 647 goat antirabbit IgG (A27040; Invitrogen); Alexa Fluor 488 goat antiguinea pig IgG (A-11073; Invitrogen); Alexa Fluor 555 goat antiguinea pig IgG (A-21435; Invitrogen); and Alexa Fluor 555 goat antirabbit IgG (A-21428; Invitrogen).

Primary astrocytic culture and transfection

Astrocytes were prepared from the brain of *Drd2*-deficient and wild-type C57BL/6 mice at postnatal days 0–1, as previously described (Menet et al., 2001). The neonatal brains were dissociated, and cells were plated at a density of 5×10^7 cells/75 cm^2 PLL-coated flask (Corning) in DMEM containing 10% FBS. Culture media were changed 24 h later to complete medium and subsequently once every 3 d. Cultures were shaken to remove the top layer of cells sitting over the astroglial monolayer to yield astrocytes with a flat morphology between day 7 and 9. Before experimental treatments, astrocytic cultures were passaged once. Cells were allowed to reach 90% confluence. Cultures were transfected with LV or treated with compounds at various concentrations for the indicated incubation times. Untreated cells were included as controls in all experiments.

EAE

EAE was induced as previously described (Ousman et al., 2007). Briefly, recipient mice were subcutaneously injected with myelin oligodendrocyte glycoprotein (MOG_{35-55}, 200 mg/animal) emulsified in CFA containing 5 mg/ml killed *Mycobacterium tuberculosis* (DIFCO), and i.p. injected with pertussis toxin (400 ng/animal; Sigma-Aldrich) on day 0 and 2. Clinical scoring of EAE was undertaken using a five-point scale with half-point gradations (Guo et al., 2019).

Knockdown of PTS in astrocytes

Two siRNAs targeting mouse Pts were designed (Pts-86 sense, 5′-CCCAUCUCUGAGCGAUGAATT-3′, antisense, 5′-UUCAUCGCUCAGAGAUGGGTT-3′; Pts-223 sense, 5′-CCGACCUCAAAGAAUACAUTT-3′, antisense, 5′-AUGUAUUCUUUGAGGUCGGTT-3′; nonsilencing control sense, 5′-UUCUCCGAACGUGUCACGUTT-3′, antisense, 5′-ACGUGACACGUUCGGAGAATT-3′). The preparation of miR-30–based shRNA according to the siRNA sequence was performed as previously described (Chang et al., 2013). The pLenti-GFAP-EGFP-mir30-shAct1 vector (Yan et al., 2012) was a gift from Ya-ping Yan. The cDNA of mouse Pts was amplified and subcloned into pLenti vector (cat. #H139; OBIO) for overexpression.

Histological analysis

Mouse spinal cords were removed and were fixed in 4% PFA overnight. Paraffin-embedded tissue was cut at the thickness of 5 mm, and then stained with hematoxylin and eosin. The severity of demyelination was analyzed by using Luxol Fast Blue/H&E staining.

Isolation of total RNA, RNA-seq analysis, and bioinformatics analysis

Isolation of total RNA, RNA-seq analysis, and bioinformatics analysis was performed as described previously (Zhang et al., 2019). Briefly, the spinal cords of adult mice were homogenized in TRIzol reagent (Invitrogen). Total RNA was purified, and cDNA was synthesized. Sequencing libraries were generated

using NEB Next Ultra RNA Library Prep Kit for Illumina (NEB) following the manufacturer's recommendations, and index codes were added to attribute sequences to each sample.

DRD2 agonists/antagonist treatment

Drd2^{Thy1} cKO mice were administrated with DRD2 antagonist DHCB (20 mg/kg, gift from X.M. Liang; Zhang et al., 2014), or L-741,626 (5 mg/kg, Cat#1003; TOCRIS) i.p. and once daily, starting from day 2 to day 30 following EAE induction with MOG_{35-55}. Some wild-type animals received with either combination of DRD2 agonists (quinpirole, 4 mg/kg, S7395; Sigma-Aldrich, and rotigotine, 2 mg/kg, R3030; Sigma-Aldrich) or antagonists (haloperidol, 4 mg/kg, H1512; Sigma-Aldrich, and spiperone, 2 mg/kg) or vehicle (0.12 M HCl and 2.5% dimethyl sulfoxide in saline). These mice were administrated i.p. daily starting from day 14 to day 17 following EAE induction with MOG_{35-55}.

RNA isolation and quantitative PCR (qPCR)

RNA isolation and qPCR were performed as previously described (Shao et al., 2013). β-actin was used as an internal control gene. qPCR primers were designed using primer designing tool at NCBI and their sequences primer sequences are as follows: PTS, forward, 5′-GGCCACGGGCACAACTATAA-3′, reverse, 3′-AAG TACGGCACATCCAGGTC-3′; CCL2, forward, 5′-GAGCAGTGT GGAGTTCGAGG-3′, reverse, 5′-CCGGATCTAGGCAGGTTTGA-3′; CXCL1, forward, 5′-CTTGCCTTGACCCTGAAGCTC-3′, reverse, 5′-AGCAGTCTGTCTTCTTTCTCCGT-3′; CXCL2, forward, 5′-CCCCCTGGTTCAGAAAATCA-3′, reverse, 5′-GCTCCTCCTTTC CAGGTCAGT-3′; IL-6, forward, 5′-ACACATGTTCTCTGGGAA ATCGT-3′, reverse, 5′-AAGTGCATCATCGTTGTTCATACA-3′; IL-4, forward, 5′-TCCTCACAGCAACGAAGAAC-3′, reverse, 5′-CTGCAGCTCCATGAGAACAC-3′; IL-10, forward, 5′-ACTGCT ATGCTGCCTGCTCT-3′, reverse, 5′-CCTGCATTAAGGAGTCGG TTA-3′; IL-17, forward, 5′-AGCTTCATCTGTGTCTCTGAT-3′, reverse, 5′-GAGTTAAAGACTTTGAGGTTGA-3′; INF-g, forward, 5′-CATGGCTGTTTCTGGCTGTT-3′, reverse, 5′-TGTTGCTGA TGGCCTGATTGT-3′; LY6C, forward, 5′-CTGTGCCTGCAACCT TGTCT-3′, reverse, 5′-TGCAGAATCCATCAGAGGCG-3′; F4/80, forward, 5′-GATGACCACACTTCCCACCC-3′, reverse, 5′-GAC TGAGTTAGGACCACAAGGT-3′; CXCL9, forward, 5′-TGCACG ATGCTCCTGCA-3′, reverse, 5′-AGGTCTTTGAGGGATTTGTAG TG-3′; CXCL10, forward, 5′-CTCATCCTGCTGGGTCTGAG-3′, reverse, 5′-CCTATGTCGCAGCCGTTACTC-3′; CXCL11, forward, 5′-AACAGGGGCGCTGTCTTT-3′, reverse, 5′-CTTTGTCGCAGC CGTTACTC-3′; CXCL12, forward, 5′-AACCAGTCAGCCTGAGCT ACC-3′, reverse, 5′-CTGAAGGGCACAGTTTGGAG-3′; MMP3, forward, 5′-GTTGGAGATGACAGGGAAGC-3′, reverse, 5′-CGA ACCTGGGAAGGTACTGA-3′; MMP9, forward, 5′-CCAGATGAT GGGAGAGAAGC-3′, reverse, 5′-GGCCTTTAGTGTCTGGCTGT-3′; CCL20, forward, 5′-GTGGCAAGCGTCTGCTCT-3′, reverse, 5′-TGTACGAGAGGCAACAGTCG-3′; GM-CSF, forward, 5′-GTGGTC TACAGCCTCTCAGCA-3′, reverse, 5′-GCATGTCATCCAGGAGGT TC-3′; TNF-α, forward, 5′-ACGTCGTAGCAAACCACCAA-3′, reverse, 5′-ATAGCAAATCGGCTGACGGT-3′; SPP1, forward, 5′-CAGAATCTCCTTGCGCCACA-3′, reverse, 5′-ATGTGGTCATGG CTTTCATTGG-3′; H2-AA, forward, 5′-CTGTGGAGGTGAAGA CGACA-3′, reverse, 5′-GTGTACTGGCCAATGTCTCCA-3′; CD3, forward, 5′-GTCCGCCATCTTGGTAGAGAG-3′, reverse, 5′-CAA TGTTCTCGGCATCGTCC-3′; CD4, forward, 5′-TGTCACTCAAGG GAAGACGC-3′, reverse, 5′-CCTTTCTCCCATGCCCCTTT-3′; CD8, forward, 5′-CACCCTACCGGGACATCTCA-3′, reverse, 5′-CTC TGAAGGTCTGGGCTTGC-3′; CD45, forward, 5′-TAAGACAGA GTGCAAAGGAGACC-3′, reverse, 5′-GGTAGCATCACTGGGTGT AGG-3′.

RNA-seq and analysis

Sample preparation for RNA-seq analysis was carried out as described previously (Zhang et al., 2019). In brief, the spinal cord of 2∼3-mo-old *Drd2* cKO mice and littermate control were homogenized in TRIzol reagent (Invitrogen) on day 17 after EAE induction. The RNA sequencing library was made using NEBNext Ultra RNA Library Prep Kit for Illumina (NEB). RNA-seq was performed on Novaseq 6000 (illumine, Inc.). Data quality check was done by CASAVA. De-multiplexing was performed with HISAT2 v2.0.5 program. DESeq2 (1.16.1) was used to identify the differentially expressed genes. Meanwhile, Benjamini and Hochberg program were used to control false discovery rate. The GO enrichment and KEGG pathway enrichment were performed using ClusterProfiler R program. GSEA was analyzed by GSEA analyses program (http://www.broadinstitute.org/gsea/index.jsp). These procedures were performed in Novogene.

Establishment of HEK293T cells stably expressing NF-κB luciferase reporter gene

HEK293T cells (Cell Bank, Chinese Academy of Sciences) were cotransfected with pLenti-NF-κB-GFP-luciferase reporter gene (Pessara and Koch, 1990; Baeuerle, 1998; NF-κB-Luc-Blastincidin [V3], Ji Manchu Biotechnology), and DRD2 or PTS. Cells transfected with pLenti-Flag-2A-GFP served as negative control. The GFP$^+$ clones were isolated and expanded following the cotransfection by using flow cytometry. Luciferase activity was measured using Ensight (PerkinElmer).

Flow cytometry analysis

Single-cell suspensions of the lymph nodes, spleen or brains, and spinal cords were collected from MOG_{35-55}–immunized mice. Dead cells were stained with a live and dead violet viability kit (Invitrogen) and were gated out in the analysis. Antibodies used for flow cytometry were purchased from eBioscience: anti-CD45, anti-CD4, anti-CD8, anti-CD25, anti-CD11b, anti-Gr1, anti-Foxp3, anti-CD69, anti-IL17A, and anti–IFN-g (1:1,000). For intracellular cytokine staining, the CNS-infiltrating T cells were stimulated for 4 h with PMA plus ionomycin in the presence of monensin and then subjected to intracellular IFN-γ, IL-17a staining, and flow cytometry analysis. For nuclear staining, cells were fixed and permeablized using a Mouse Regulatory T Cell Staining Kit (Thermo Fisher Scientific). Flow cytometry data were collected using the CytoFLEX LX Flow Cytometer (Beckman Coulter).

Viral injection

Lentiviral vectors knocking down PTS or encoding PTS were prepared by Shanghai OBIO. The titers of the packaged virus in this study were at least 1 × 10^8 TU/ml. Mice were deeply

anesthetized with pentobarbital sodium (30 mg/kg, i.p.) and placed in a stereotaxic frame. A total of 3 × 10^6 TU of LV (Lv-GFABCID-GFP-shNC, Lv-GFABC1D-GFP-shPTS) was injected unilaterally into the lateral ventricle using Hamilton syringe. Mice were then subjected to EAE 3–7 d after the surgery.

Statistical analysis

Statistical analysis was performed using GraphPad software (GraphPad Prism v8.0; GraphPad Software). Data are presented as mean ± SEM. The statistics were carried by using a two-tailed unpaired *t* test or a two-sided one-/two-way ANOVA followed by either Dunnet test or Student–Newman–Keul's test (as a post hoc test). $P < 0.05$ was considered as significant in statistics. P values are *, $P < 0.05$; **, $P < 0.01$; and ***, $P < 0.001$.

Online supplemental material

Fig. S1 shows microglia activation and demyelination in the spinal cord of *Drd2*^{Thy1} cKO and control mice following EAE induction. Fig. S2 shows selective ablation of *Drd2* in astrocytes suppresses inflammatory response in EAE. Fig. S3 shows flow cytometry and qPCR analysis of CNS tissue, lymph nodes, and spleen of *Drd2* cKO mice in EAE. Fig. S4 shows RNA-seq analysis of the spinal cord of *Drd2*^{mGFAP} cKO mice in EAE. Fig. S5 shows the effects of dopamine receptor agonists/antagonists on the activation of NF-κB pathway in DRD2-expressing HEK293T cells and during the EAE. Table S1 shows the summary of the demographic and clinicopathological data on the seven MS and seven nondemented controls used for Western blot analysis in this study. Table S2 shows the summary of the demographic and clinicopathological data on the five MS and five control cases used for immunofluorescent staining in this study.

Data availability

The data that support the findings of this study are available from the corresponding author upon reasonable request. Raw data files of the RNA-seq have been deposited in Gene Expression Omnibus under accession number GSE205292.

Acknowledgments

We thank Ms. Y.D. Li and J.C. Hou for excellent assistance in genotyping; Dr. Y.C. Qian (Shanghai Institute of Nutrition and Health, Chinese Academy of Sciences, Shanghai, China) for CD4-Cre Tg mice; Dr. M. Brenner (University of Alabama, Birmingham, AL) for the GFABC1D promoter (through the Alabama Neuroscience Blueprint Core, National Institutes of Health grants NS39055 and NS057098). We also thank Dr. Q. Hu and his colleagues from the Core Facility at ION for their technical support in confocal microscopy, and image acquisition/analyses.

This work was supported by grants from the Ministry of Science and Technology of China (2020YFC2002800), the Natural Science Foundation of China (U1801681), Strategic Priority Research Program of Chinese Academy of Science (XDB32020100), Shanghai Municipal Science and Technology Major Project (2018SHZDZX05), Key Realm R&D Program of Guangdong Province (2018B030337001), and Innovative Research Team of High-Level Local Universities in Shanghai.

Author contributions: S.-z. Lu, Y. Wu, and Y.-s. Guo conducted most of the experiments and the data analysis; P.-z. Liang contributed to part of the experiments; S. Yin conducted FACS analysis and contributed to discussion; Y.-q. Yin contributed to the cell culture; X.-l. Zhang, Y.-F. Liu, and X.-m. Liang provided DHCB and other DRD2 antagonists and contributed to discussion; H.-y. Wang and Y.-c. Xiao contributed to discussion. J.-w. Zhou supervised the project and wrote the manuscript. All authors read and approved the final manuscript.

Disclosures: The authors declare no competing interests exist.

Submitted: 8 May 2021
Revised: 10 December 2021
Accepted: 8 June 2022

References

Badawi, A.H., P. Kiptoo, W.T. Wang, I.Y. Choi, P. Lee, C.M. Vines, and T.J. Siahaan. 2012. Suppression of EAE and prevention of blood-brain barrier breakdown after vaccination with novel bifunctional peptide inhibitor. *Neuropharmacology*. 62:1874–1881. https://doi.org/10.1016/j.neuropharm.2011.12.013

Baecher-Allan, C., B.J. Kaskow, and H.L. Weiner. 2018. Multiple sclerosis: Mechanisms and immunotherapy. *Neuron*. 97:742–768. https://doi.org/10.1016/j.neuron.2018.01.021

Baeuerle, P.A. 1998. Pro-inflammatory signaling: Last pieces in the NF-kappaB puzzle?. *Curr. Biol.* 8:R19–R22. https://doi.org/10.1016/s0960-9822(98)70010-7

Baranzini, S.E., J. Mudge, J.C. Van velkinburgh, P. Khankhanian, I. Khrebtukova, N.A. Miller, L. Zhang, A.D. Farmer, C.J. Bell, R.W. Kim, et al. 2010. Genome, epigenome and RNA sequences of monozygotic twins discordant for multiple sclerosis. *Nature*. 464:1351–1356. https://doi.org/10.1038/nature08990

Beaulieu, J.M., and R.R. Gainetdinov. 2011. The physiology, signaling, and pharmacology of dopamine receptors. *Pharmacol. Rev.* 63:182–217. https://doi.org/10.1124/pr.110.002642

Bennett, J., J. Basivireddy, A. Kollar, K.E. Biron, P. Reickmann, W.A. Jefferies, and S. Mcquaid. 2010. Blood-brain barrier disruption and enhanced vascular permeability in the multiple sclerosis model EAE. *J. Neuroimmunol.* 229:180–191. https://doi.org/10.1016/j.jneuroim.2010.08.011

Besser, M.J., Y. Ganor, and M. Levite. 2005. Dopamine by itself activates either D2, D3 or D1/D5 dopaminergic receptors in normal human T-cells and triggers the selective secretion of either IL-10, TNFalpha or both. *J. Neuroimmunol.* 169:161–171. https://doi.org/10.1016/j.jneuroim.2005.07.013

Brosnan, C.F., and C.S. Raine. 2013. The astrocyte in multiple sclerosis revisited. *Glia*. 61:453–465. https://doi.org/10.1002/glia.22443

Burguillos, M.A., T. Deierborg, E. Kavanagh, A. Persson, N. Hajji, A. Garcia-quintanilla, J. Cano, P. Brundin, E. Englund, J.L. Venero, and B. Joseph. 2011. Caspase signalling controls microglia activation and neurotoxicity. *Nature*. 472:319–324. https://doi.org/10.1038/nature09788

Cai, L., M. Bian, M. Liu, Z. Sheng, H. Suo, Z. Wang, F. Huang, and J. Fei. 2011. Ethanol-induced neurodegeneration in NRSF/REST neuronal conditional knockout mice. *Neuroscience*. 181:196–205. https://doi.org/10.1016/j.neuroscience.2011.02.059

Campsall, K.D., C.J. Mazerolle, Y. De Repentingy, R. Kothary, and V.A. Wallace. 2002. Characterization of transgene expression and Cre recombinase activity in a panel of Thy-1 promoter-Cre transgenic mice. *Dev. Dynam.* 224:135–143. https://doi.org/10.1002/dvdy.10092

Chabas, D., S.E. Baranzini, D. Mitchell, C.C. Bernard, S.R. Rittling, D.T. Denhardt, R.A. Sobel, C. Lock, M. Karpuj, R. Pedotti, et al. 2001. The influence of the proinflammatory cytokine, osteopontin, on autoimmune demyelinating disease. *Science*. 294:1731–1735. https://doi.org/10.1126/science.1062960

Chang, K., K. Marran, A. Valentine, and G.J. Hannon. 2013. Creating an miR30-based shRNA vector. *Cold Spring Harb. Protoc.* 2013:631–635. https://doi.org/10.1101/pdb.prot075853

Dobryakova, E., J. Deluca, H.M. Genova, and G.R. Wylie. 2013. Neural correlates of cognitive fatigue: Cortico-striatal circuitry and effort-reward imbalance. *J. Int. Neuropsychol. Soc.* 19:849–853. https://doi.org/10.1017/S1355617713000684

Dobryakova, E., H.M. Genova, J. Deluca, and G.R. Wylie. 2015. The dopamine imbalance hypothesis of fatigue in multiple sclerosis and other neurological disorders. *Front. Neurol.* 6:52. https://doi.org/10.3389/fneur.2015.00052

Engstrom, M., G. Flensner, A.M. Landtblom, A.C. Ek, and T. Karlsson. 2013. Thalamo-striato-cortical determinants to fatigue in multiple sclerosis. *Brain Behav.* 3:715–728. https://doi.org/10.1002/brb3.181

Franscini, N., N. Blau, R.B. Walter, A. Schaffner, and G. Schoedon. 2003. Critical role of interleukin-1beta for transcriptional regulation of endothelial 6-pyruvoyltetrahydropterin synthase. *Arterioscler. Thromb. Vasc. Biol.* 23:e50–e53. https://doi.org/10.1161/01.ATV.0000099785.65848.F1

Glass, C.K., K. Saijo, B. Winner, M.C. Marchetto, and F.H. Gage. 2010. Mechanisms underlying inflammation in neurodegeneration. *Cell.* 140:918–934. https://doi.org/10.1016/j.cell.2010.02.016

Gregorian, C., J. Nakashima, J. Le Belle, J. Ohab, R. Kim, A. Liu, K.B. Smith, M. Groszer, A.D. Garcia, M.V. Sofroniew, et al. 2009. Pten deletion in adult neural stem/progenitor cells enhances constitutive neurogenesis. *J. Neurosci.* 29:1874–1886. https://doi.org/10.1523/JNEUROSCI.3095-08.2009

Grossman, R.I., F. Gonzalez-scarano, S.W. Atlas, S. Galetta, and D.H. Silberberg. 1986. Multiple sclerosis: Gadolinium enhancement in MR imaging. *Radiology*. 161:721–725. https://doi.org/10.1148/radiology.161.3.3786722

Guo, Y.S., P.Z. Liang, S.Z. Lu, R. Chen, Y.Q. Yin, and J.W. Zhou. 2019. Extracellular αB-crystallin modulates the inflammatory responses. *Biochem. Biophys. Res. Commun.* 508:282–288. https://doi.org/10.1016/j.bbrc.2018.11.024

Hayden, M.S., and S. Ghosh. 2012. NF-κB, the first quarter-century: Remarkable progress and outstanding questions. *Genes Dev.* 26:203–234. https://doi.org/10.1101/gad.183434.111

Hendrickx, D.A.E., J. van Scheppingen, M. van der Poel, K. Bossers, K.G. Schuurman, C.G. van Eden, E.M. Hol, J. Hamann, and I. Huitinga. 2017. Gene expression profiling of multiple sclerosis pathology identifies early patterns of demyelination surrounding chronic active lesions. *Front. Immunol.* 8:1810. https://doi.org/10.3389/fimmu.2017.01810

Hill, M.P., P. Ravenscroft, S.G. Mcguire, J.M. Brotchie, A.R. Crossman, C. Rochat, and M.J. Millan. 2006. Antiparkinsonian effects of the novel D3/D2 dopamine receptor agonist, S32504, in MPTP-lesioned marmosets: Mediation by D2, not D3, dopamine receptors. *Mov. Disord.* 21:2090–2095. https://doi.org/10.1002/mds.21106

Hur, E.M., S. Youssef, M.E. Haws, S.Y. Zhang, R.A. Sobel, and L. Steinman. 2007. Osteopontin-induced relapse and progression of autoimmune brain disease through enhanced survival of activated T cells. *Nat. Immunol.* 8:74–83. https://doi.org/10.1038/ni1415

Huynh, J.L., P. Garg, T.H. Thin, S. Yoo, R. Dutta, B.D. Trapp, V. Haroutunian, J. Zhu, M.J. Donovan, A.J. Sharp, and P. Casaccia. 2014. Epigenome-wide differences in pathology-free regions of multiple sclerosis-affected brains. *Nat. Neurosci.* 17:121–130. https://doi.org/10.1038/nn.3588

Kang, Z., C. Wang, J. Zepp, L. Wu, K. Sun, J. Zhao, U. Chandrasekharan, P.E. Dicorleto, B.D. Trapp, R.M. Ransohoff, and X. Li. 2013. Act1 mediates IL-17-induced EAE pathogenesis selectively in NG2+ glial cells. *Nat. Neurosci.* 16:1401–1408. https://doi.org/10.1038/nn.3505

Kavanagh, E., J. Rodhe, M.A. Burguillos, J.L. Venero, and B. Joseph. 2014. Regulation of caspase-3 processing by cIAP2 controls the switch between pro-inflammatory activation and cell death in microglia. *Cell Death Dis.* 5:e1565. https://doi.org/10.1038/cddis.2014.514

Laufs, S., N. Blau, and B. Thony. 1998. Retrovirus-mediated double transduction of the GTPCH and PTPS genes allows 6-pyruvoyltetrahydropterin synthase-deficient human fibroblasts to synthesize and release tetrahydrobiopterin. *J. Neurochem.* 71:33–40. https://doi.org/10.1046/j.1471-4159.1998.71010033.x

Lee, Y., A. Messing, M. Su, and M. Brenner. 2008. GFAP promoter elements required for region-specific and astrocyte-specific expression. *Glia*. 56:481–493. https://doi.org/10.1002/glia.20622

Li, A., H. Guo, X. Luo, J. Sheng, S. Yang, Y. Yin, J. Zhou, and J. Zhou. 2006. Apomorphine-induced activation of dopamine receptors modulates FGF-2 expression in astrocytic cultures and promotes survival of dopaminergic neurons. *FASEB J.* 20:1263–1265. https://doi.org/10.1096/fj.05-5510fje

Li, L., H. Zhang, and A.S. Verkman. 2009. Greatly attenuated experimental autoimmune encephalomyelitis in aquaporin-4 knockout mice. *BMC Neurosci.* 10:94. https://doi.org/10.1186/1471-2202-10-94

Liddelow, S.A., K.A. Guttenplan, L.E. Clarke, F.C. Bennett, C.J. Bohlen, L. Schirmer, M.L. Bennett, A.E. Munch, W.S. Chung, T.C. Peterson, et al. 2017. Neurotoxic reactive astrocytes are induced by activated microglia. *Nature*. 541:481–487. https://doi.org/10.1038/nature21029

Lindvall, O., A. Björklund, and G. Skagerberg. 1983. Dopamine-containing neurons in the spinal cord: Anatomy and some functional aspects. *Ann. Neurol.* 14:255–260. https://doi.org/10.1002/ana.410140302

Linscheid, P., A. Schaffner, N. Blau, and G. Schoedon. 1998. Regulation of 6-pyruvoyltetrahydropterin synthase activity and messenger RNA abundance in human vascular endothelial cells. *Circulation*. 98:1703–1706. https://doi.org/10.1161/01.cir.98.17.1703

Mattson, M.P., and S. Camandola. 2001. NF-kappaB in neuronal plasticity and neurodegenerative disorders. *J. Clin. Invest.* 107:247–254. https://doi.org/10.1172/JCI11916

Mayo, L., S.A. Trauger, M. Blain, M. Nadeau, B. Patel, J.I. Alvarez, I.D. Mascanfroni, A. Yeste, P. Kivisakk, K. Kallas, et al. 2014. Regulation of astrocyte activation by glycolipids drives chronic CNS inflammation. *Nat. Med.* 20:1147–1156. https://doi.org/10.1038/nm.3681

Melnikov, M., V. Rogovskii, A. Boyko, and M. Pashenkov. 2020. Dopaminergic therapeutics in multiple sclerosis: Focus on Th17-cell functions. *J. Neuroimmune Pharmacol.* 15:37–47. https://doi.org/10.1007/s11481-019-09852-3

Menet, V., M. Gimenez Y Ribotta, N. Chauvet, M.J. Drian, J. Lannoy, E. Colucci-Guyon, and A. Privat. 2001. Inactivation of the glial fibrillary acidic protein gene, but not that of vimentin, improves neuronal survival and neurite growth by modifying adhesion molecule expression. *J. Neurosci.* 21:6147–6158. https://doi.org/10.1523/jneurosci.21-16-06147.2001

Miller, S.D., and W.J. Karpus. 2007. Experimental autoimmune encephalomyelitis in the mouse. *Curr. Protoc. Immunol.* Chapter 15:Unit 15.1. https://doi.org/10.1002/0471142735.im1501s77

Mirshafiey, A., B. Asghari, G. Ghalamfarsa, F. Jadidi-Niaragh, and G. Azizi. 2014. The significance of matrix metalloproteinases in the immunopathogenesis and treatment of multiple sclerosis. *Sultan Qaboos Univ. Med. J.* 14:e13–e25. https://doi.org/10.12816/0003332

Mladinov, M., D. Mayer, L. Brčić, E. Wolstencroft, N.T. Man, I. Holt, P.R. Hof, G.E. Morris, and G. Šimić. 2010. Astrocyte expression of D2-lIke DopAmIne receptors in the prefrontAl cortex. *Transl. Neurosci.* 1:238–243. https://doi.org/10.2478/v10134-010-0035-6

Ousman, S.S., B.H. Tomooka, J.M. Van Noort, E.F. Wawrousek, K.C. O'connor, D.A. Hafler, R.A. Sobel, W.H. Robinson, and L. Steinman. 2007. Protective and therapeutic role for alphaB-crystallin in autoimmune demyelination. *Nature*. 448:474–479. https://doi.org/10.1038/nature05935

Pacheco, R., C.E. Prado, M.J. Barrientos, and S. Bernales. 2009. Role of dopamine in the physiology of T-cells and dendritic cells. *J. Neuroimmunol.* 216:8–19. https://doi.org/10.1016/j.jneuroim.2009.07.018

Pardini, M., L. Bonzano, G.L. Mancardi, and L. Roccatagliata. 2010. Frontal networks play a role in fatigue perception in multiple sclerosis. *Behav. Neurosci.* 124:329–336. https://doi.org/10.1037/a0019585

Paty, D.W., and H. McFarland. 1998. Magnetic resonance techniques to monitor the long term evolution of multiple sclerosis pathology and to monitor definitive clinical trials. *J. Neurol. Neurosurg. Psychiatry*. 64:S47–S51

Pessara, U., and N. Koch. 1990. Tumor necrosis factor alpha regulates expression of the major histocompatibility complex class II-associated invariant chain by binding of an NF-kappa B-like factor to a promoter element. *Mol. Cell Biol.* 10:4146–4154. https://doi.org/10.1128/mcb.10.8.4146-4154.1990

Reich, D.S., C.F. Lucchinetti, and P.A. Calabresi. 2018. Multiple sclerosis. *N. Engl. J. Med.* 378:169–180. https://doi.org/10.1056/NEJMra1401483

Rothhammer, V., D.M. Borucki, E.C. Tjon, M.C. Takenaka, C.C. Chao, A. Ardura-Fabregat, K.A. De Lima, C. Gutierrez-Vazquez, P. Hewson, O. Staszewski, et al. 2018. Microglial control of astrocytes in response to microbial metabolites. *Nature*. 557:724–728. https://doi.org/10.1038/s41586-018-0119-x

Shao, W., S.Z. Zhang, M. Tang, X.H. Zhang, Z. Zhou, Y.Q. Yin, Q.B. Zhou, Y.Y. Huang, Y.J. Liu, E. Wawrousek, et al. 2013. Suppression of neuroinflammation by astrocytic dopamine D2 receptors via αB-crystallin. *Nature*. 494:90–94. https://doi.org/10.1038/nature11748

Sofroniew, M.V. 2020. Astrocyte reactivity: Subtypes, states, and functions in CNS innate immunity. *Trends Immunol.* 41:758–770. https://doi.org/10.1016/j.it.2020.07.004

Sofroniew, M.V., and H.V. Vinters. 2010. Astrocytes: Biology and pathology. *Acta Neuropathol.* 119:7–35. https://doi.org/10.1007/s00401-009-0619-8

Spiegel, S., and S. Milstien. 2011. The outs and the ins of sphingosine-1-phosphate in immunity. *Nat. Rev. Immunol.* 11:403–415. https://doi.org/10.1038/nri2974

Sun, Y., Q. Wang, Y. Wang, W. Ren, Y. Cao, J. Li, X. Zhou, W. Fu, and J. Yang. 2021. Sarm1-mediated neurodegeneration within the enteric nervous system protects against local inflammation of the colon. *Protein Cell*. 12: 621–638. https://doi.org/10.1007/s13238-021-00835-w

Surmeier, D.J. 2018. Determinants of dopaminergic neuron loss in Parkinson's disease. *FEBS J*. 285:3657–3668. https://doi.org/10.1111/febs.14607

Traugott, U. 1987. Multiple sclerosis: Relevance of class I and class II MHC-expressing cells to lesion development. *J. Neuroimmunol.* 16:283–302. https://doi.org/10.1016/0165-5728(87)90082-8

van Loo, G., R. De Lorenzi, H. Schmidt, M. Huth, A. Mildner, M. Schmidt-Supprian, H. Lassmann, M.R. Prinz, and M. Pasparakis. 2006. Inhibition of transcription factor NF-kappaB in the central nervous system ameliorates autoimmune encephalomyelitis in mice. *Nat. Immunol.* 7: 954–961. https://doi.org/10.1038/ni1372

Walker, L.A.S., J.A. Berard, L.I. Berrigan, L.M. Rees, and M.S. Freedman. 2012. Detecting cognitive fatigue in multiple sclerosis: Method matters. *J. Neurol. Sci.* 316:86–92. https://doi.org/10.1016/j.jns.2012.01.021

Wang, Q., Y. Liu, and J. Zhou. 2015. Neuroinflammation in Parkinson's disease and its potential as therapeutic target. *Transl. Neurodegener.* 4:19. https://doi.org/10.1186/s40035-015-0042-0

Wheeler, M.A., I.C. Clark, E.C. Tjon, Z. Li, S.E.J. Zandee, C.P. Couturier, B.R. Watson, G. Scalisi, S. Alkwai, V. Rothhammer, et al. 2020. MAFG-driven astrocytes promote CNS inflammation. *Nature*. 578:593–599. https://doi.org/10.1038/s41586-020-1999-0

Wheeler, M.A., and F.J. Quintana. 2019. Regulation of astrocyte functions in multiple sclerosis. *Cold Spring Harb. Perspect. Med.* 9:a029009. https://doi.org/10.1101/cshperspect.a029009

Wojkowska, D.W., P. Szpakowski, D. Ksiazek-Winiarek, M. Leszczynski, and A. Glabinski. 2014. Interactions between neutrophils, Th17 cells, and chemokines during the initiation of experimental model of multiple sclerosis. *Mediators Inflamm.* 2014:590409. https://doi.org/10.1155/2014/590409

Wu, Y., Y. Hu, B. Wang, S. Li, C. Ma, X. Liu, P.N. Moynagh, J. Zhou, and S. Yang. 2020. Dopamine uses the DRD5-ARRB2-PP2A signaling axis to block the TRAF6-mediated NF-κB pathway and suppress systemic inflammation. *Mol. Cell*. 78:42–56 e6. https://doi.org/10.1016/j.molcel.2020.01.022

Yamaguchi, H., A. Aiba, K. Nakamura, K. Nakao, H. Sakagami, K. Goto, H. Kondo, and M. Katsuki. 1996. Dopamine D2 receptor plays a critical role in cell proliferation and proopiomelanocortin expression in the pituitary. *Gene Cell.* 1:253–268. https://doi.org/10.1046/j.1365-2443.1996.d01-238.x

Yan, Y., X. Ding, K. Li, B. Ciric, S. Wu, H. Xu, B. Gran, A. Rostami, and G.X. Zhang. 2012. CNS-specific therapy for ongoing EAE by silencing IL-17 pathway in astrocytes. *Mol. Ther.* 20:1338–1348. https://doi.org/10.1038/mt.2012.12

Yang, Q.Q., and J.W. Zhou. 2019. Neuroinflammation in the central nervous system: Symphony of glial cells. *Glia*. 67:1017–1035. https://doi.org/10.1002/glia.23571

Zhang, S.Z., Q.Q. Wang, Q.Q. Yang, H.Y. Gu, Y.Q. Yin, Y.D. Li, J.C. Hou, R. Chen, Q.Q. Sun, Y.F. Sun, et al. 2019. NG2 glia regulate brain innate immunity via TGF-β2/TGFBR2 axis. *BMC Med.* 17:204. https://doi.org/10.1186/s12916-019-1439-x

Zhang, Y., C. Wang, L. Wang, G.S. Parks, X. Zhang, Z. Guo, Y. Ke, K.W. Li, M.K. Kim, B. Vo, et al. 2014. A novel analgesic isolated from a traditional Chinese medicine. *Curr. Biol.* 24:117–123. https://doi.org/10.1016/j.cub.2013.11.039

Zhu, J., Z. Hu, X. Han, D. Wang, Q. Jiang, J. Ding, M. Xiao, C. Wang, M. Lu, and G. Hu. 2018. Dopamine D2 receptor restricts astrocytic NLRP3 inflammasome activation via enhancing the interaction of beta-arrestin2 and NLRP3. *Cell Death Differ.* 25:2037–2049. https://doi.org/10.1038/s41418-018-0127-2

Supplemental material

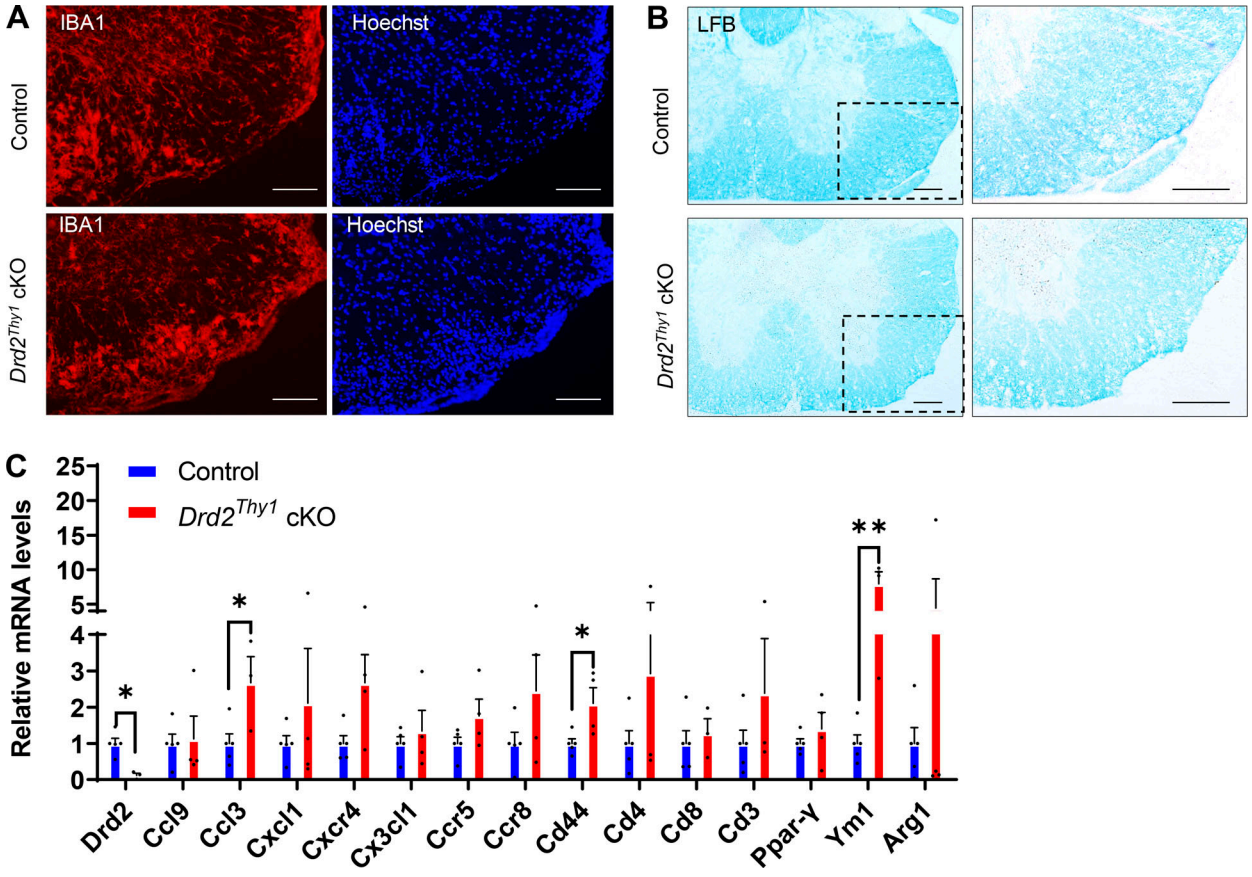

Figure S1. **Microglia activation and demyelination in the spinal cord of *Drd2*^{Thy1} cKO and control mice following EAE induction. (A)** Immunofluorescent histochemical staining for IBA1 and Hoechst in the spinal cord of *Drd2*^{Thy1} cKO mice and control on day 29 following EAE induction are shown. Scale bars, 75 µm. **(B)** Luxol fast blue staining in the spinal cord of *Drd2*^{Thy1} cKO mice and control on day 29 after EAE induction are shown. Scale bars, 100 µm. **(C)** Representative graph showing relative mRNA levels of pro-/anti-inflammatory mediators in *Drd2*^{Thy1} cKO mice and control. *n* = 3–4. Data are represented as mean ± SEM. P values are from unpaired *t* tests, *, P < 0.05; and **, P < 0.01..

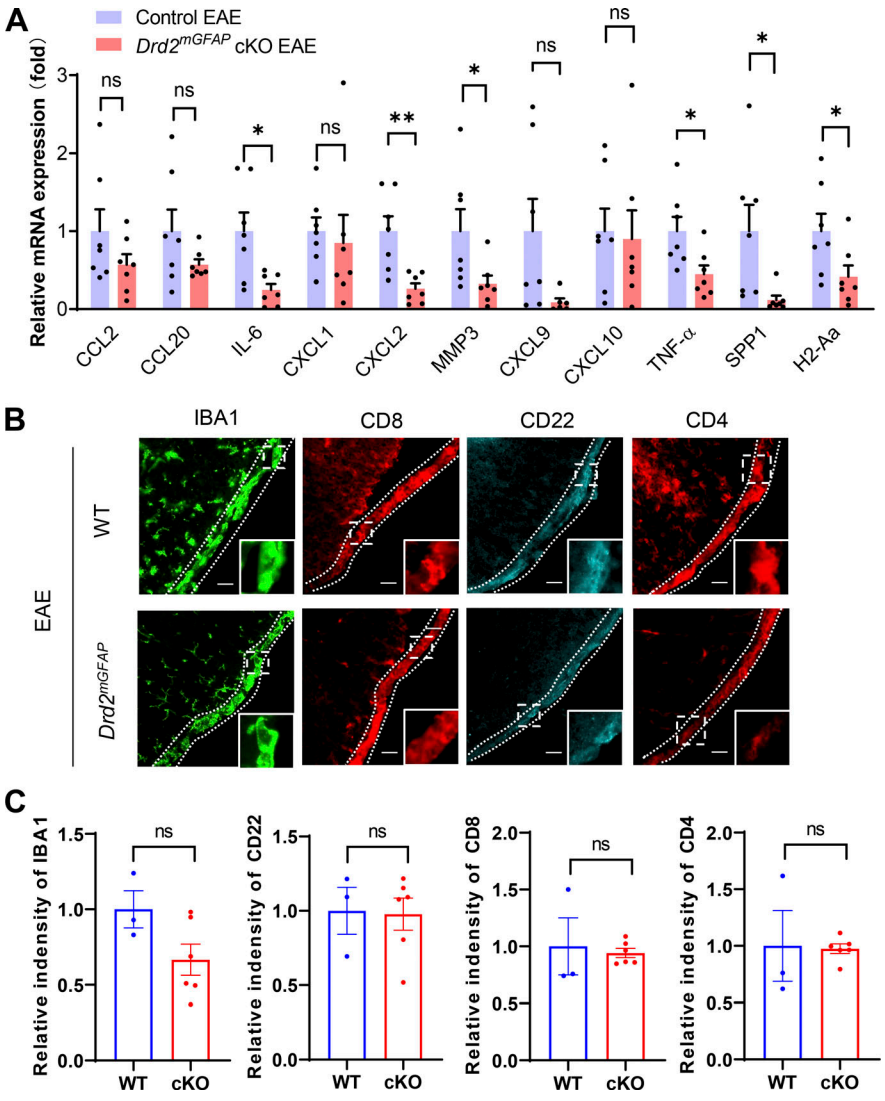

Figure S2. **Selective ablation of *Drd2* in astrocytes suppresses inflammatory response in EAE. (A)** Representative graphs showing relative mRNA levels of proinflammatory mediators in the spinal cord tissue of *Drd2*^{mGFAP} cKO and control animals on day 17 following EAE induction. *n* = 7 mice per group. **(B)** Immunofluorescent histochemical staining for IBA1, CD22, CD8, and CD4 in the leptomeninges of the spinal cord of *Drd2*^{Thy1} cKO mice and control on day 17 following EAE induction are shown. Scale bars, 20 µm. **(C)** Quantitative data of integrated intensity in areas outlined by dashed lines shown in B. *n* = 3–6 mice per group. Data are represented as mean ± SEM. P values are from unpaired *t* tests, in which ns (not significant) indicates P > 0.05; *, P < 0.05; **, P < 0.01.

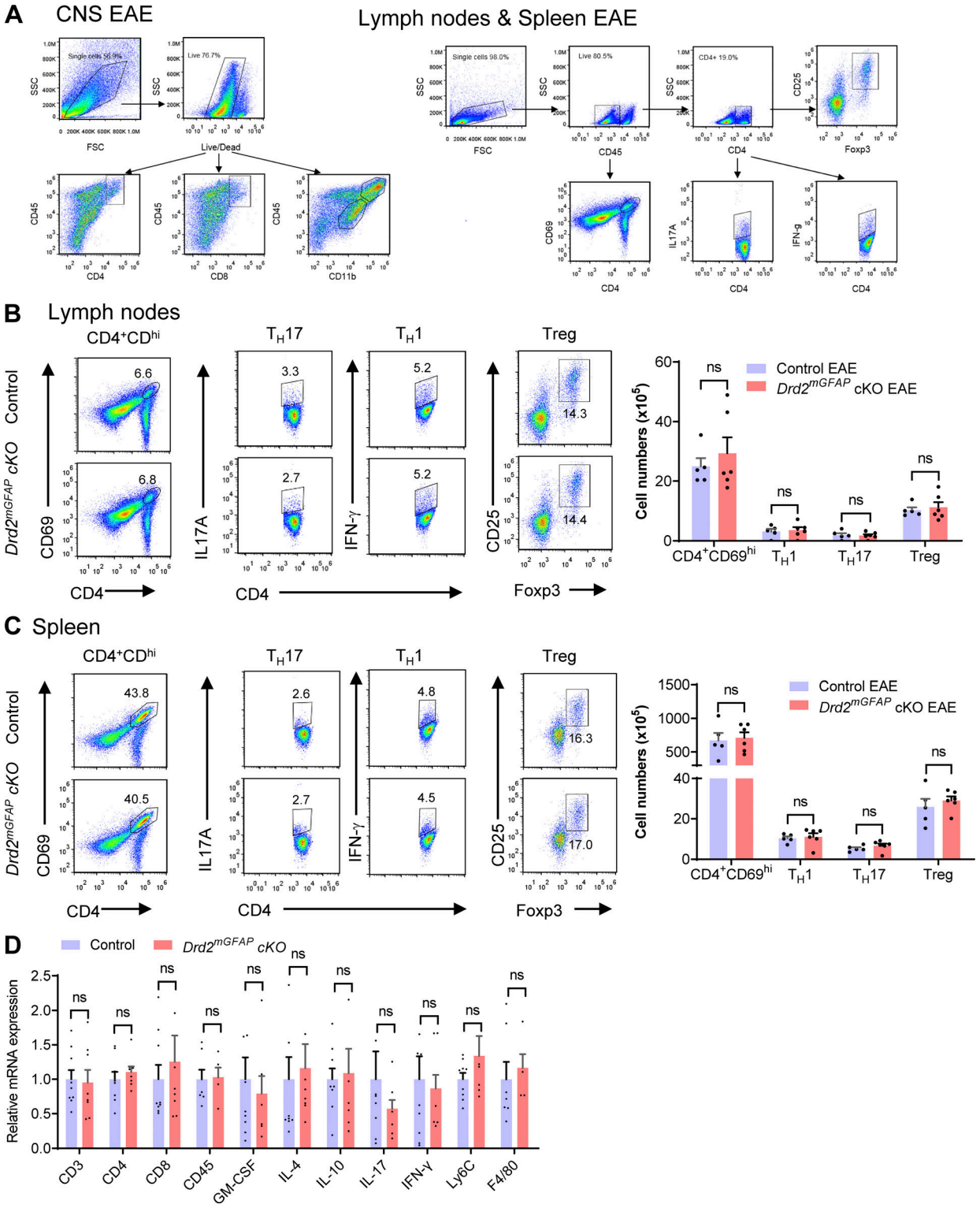

Figure S3. **Flow cytometry and qPCR analysis of CNS tissue, lymph nodes, and spleen of *Drd2* cKO mice in EAE. (A)** Gating strategies for the CNS, lymph nodes, and spleen. Please note that the data of flow cytometry analysis of CNS leukocytes are shown in Fig. 2 K. **(B and C)** Flow cytometry analysis of CD4+ T cell populations in the lymph nodes (B) or spleen (C) of MOG_{35-55}–immunized *Drd2*^{mGFAP} cKO mice and control on day 17 after EAE induction. **(D)** Representative graph showing relative mRNA levels of proinflammatory mediators in the draining lymph nodes of *Drd2*^{mGFAP} cKO and control animals on day 8 following EAE induction. $n = 6$ for cKO; $n = 4–9$ for control. Data are represented as mean ± SEM. P values are from unpaired *t* tests, in which ns (not significant) indicates $P > 0.05$.

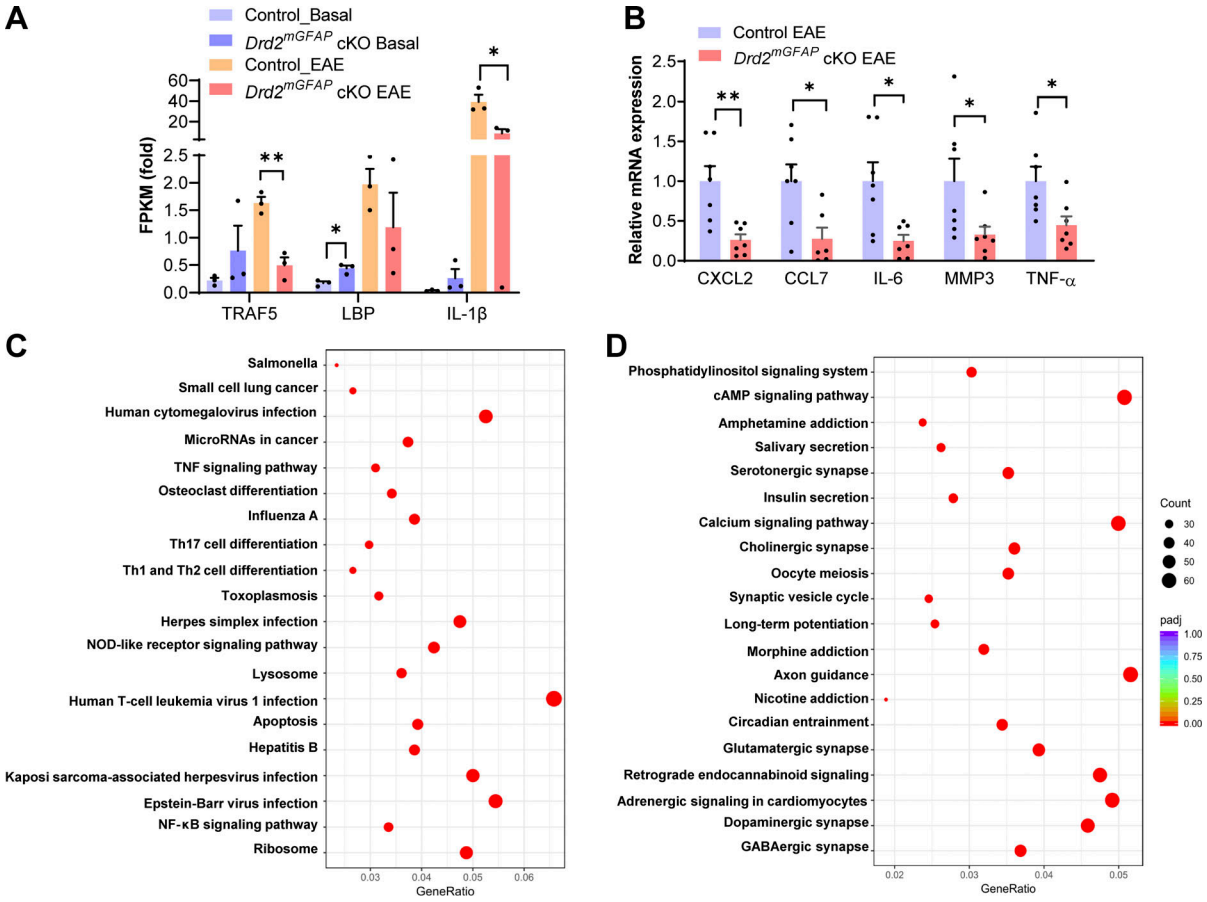

Figure S4. **RNA-seq analysis of the spinal cord of *Drd2*^{mGFAP} cKO mice in EAE. (A)** Bar graph showing the FPKM values of the indicated genes on day 17 after immunization. **(B)** Representative graph showing relative mRNA levels of proinflammatory mediators in the spinal cord of *Drd2*^{mGFAP} cKO and control animals on day 17 following EAE induction. Data are represented as mean ± SEM. n = 6 for cKO; n = 4–5 for control. **(C and D)** The top 20 enriched KEGG pathways of the downregulated (C) or upregulated (D) genes between *Drd2*^{mGFAP} cKO mice and control on day 17 after EAE induction. P values are from unpaired t tests. *, P < 0.05; **, P < 0.01.

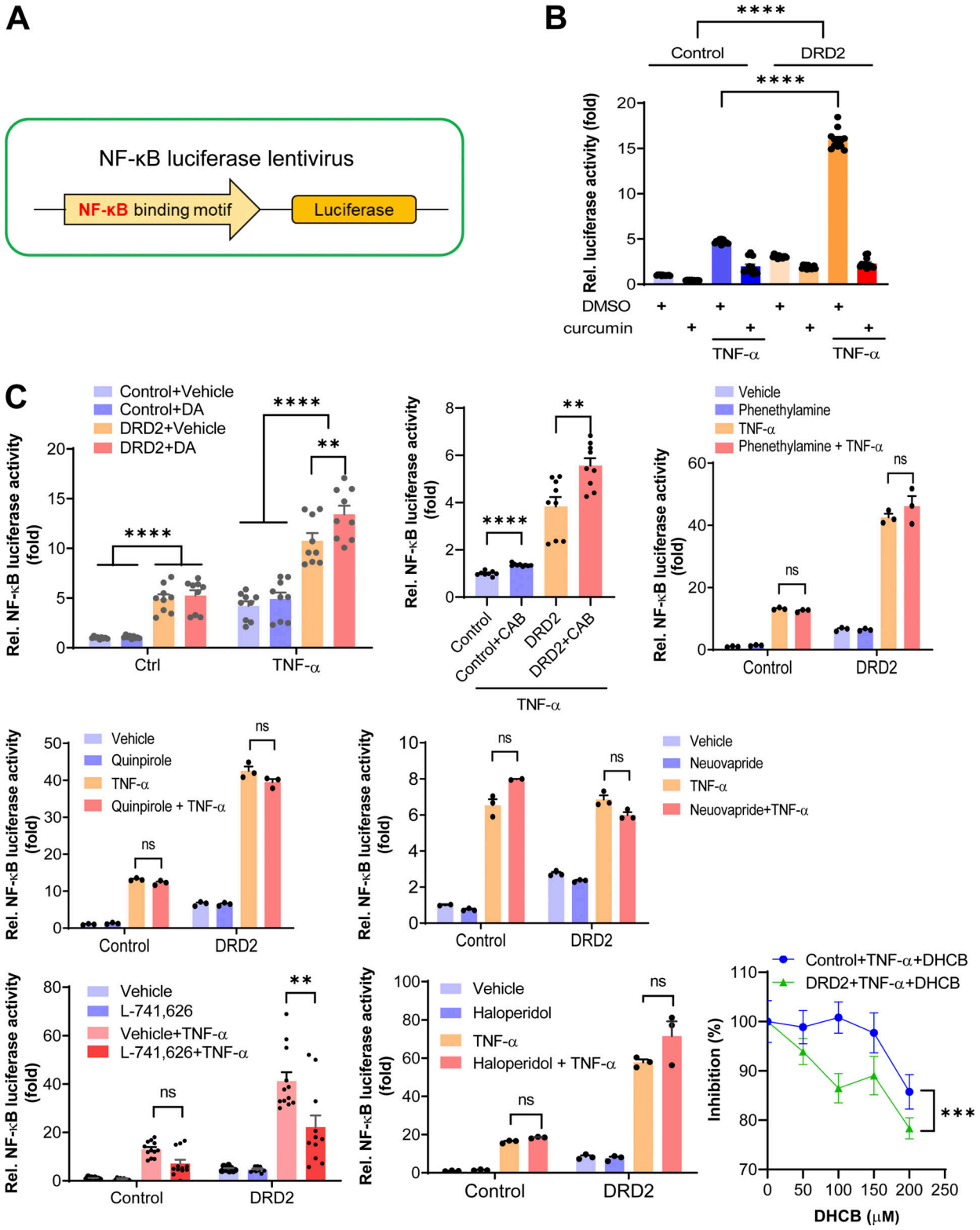

Figure S5. **Effects of dopamine receptor agonists/antagonists on the activation of NF-κB pathway in DRD2-expressing HEK293T cells and during the EAE. (A)** Schematic diagram showing the LV construct used for transfection of HEK293T cells coexpressing NF-κB luciferase reporter gene under the control of NF-κB binding motif with either DRD2 or PTS. Pretreatment with curcumin, a polyphenol isolated from the *Curcuma longa* plant, which is recognized as an anti-inflammatory agent with antioxidant activity, serves as a positive control. **(B)** Representative graph showing the NF-κB luciferase activities in the HEK293T cells coexpressing NF-κB luciferase reporter gene and DRD2, in response to treatment of TNF-α (20 ng/ml) and curcumin. **(C)** Representative graphs showing NF-κB activity in luciferase assay. Dopamine (10 μM), cabergoline (100 μM), phenethylamine (10 μM), quinpirole (10 μM), nemonapride (100 μM), haloperidol (100 μM), phenethylamine (100 μM), L-741,626 (50 μM), and TNF-α (20 ng/ml) were added in the cultures. *n* = 3 independent experiments. Data are represented as mean ± SEM. P values are from two-way ANOVA, in which **, P < 0.01 and ****, P < 0.0001.

Provided online are two tables. Table S1 shows the summary of the demographic and clinicopathological data on the seven MS and seven nondemented controls used for Western blot analysis in this study. Table S2 shows the summary of the demographic and clinicopathological data on the five MS and five control cases used for immunofluorescent staining in this study.